Computer model of IL-6 dependent rheumatoid arthritis in F759 mice

*Reiji Yamamoto[1,2], *Satoshi Yamada[3#], *Toru Atsumi[1],*Kaoru Murakami[1], *Ari Hashimoto[4], *Seiichiro Naito[1], Yuki Tanaka[1,5], Izuru Ohki[5], Yuta Shinohara[1], Norimasa Iwasaki[2], Akihiko Yoshimura[6], Jing-Jing Jiang[1], Daisuke Kamimura[1], Shintaro Hojyo[1], Shimpei I. Kubota[1], *Shigeru Hashimoto[1#], and Masaaki Murakami[1,5,7,8#]

[1]Molecular Psychoneuroimmunology, Institute of Genetic Medicine, Hokkaido University, Sapporo, Japan
[2] Department of Orthopaedic Surgery, Faculty of Medicine and Graduate School of Medicine, Hokkaido University, Sapporo, Japan
[3] Faculty of Information Science and Engineering, Okayama University of Science, Okayama, Japan
[4] Department of Molecular Biology, Hokkaido University Faculty of Medicine, Sapporo, Japan
[5] Team of Quantum immunology, Institute for Quantum Life Science, National Institute for Quantum and Radiological Science and Technology (QST), Chiba, Japan
[6] Department of Microbiology and Immunology, School of Medicine, Keio University, Tokyo, Japan
[7] Neuroimmunology, Department of Homeostatic Regulation, National Institute for Physiological Sciences, National Institutes of Natural Sciences, Aichi 444-8585, Japan
[8] Institute for Vaccine Research and Development (HU-IVReD), Hokkaido University, Sapporo 001-0020, Japan

*equal contribution
#correspondences

Address corresponded to:
Shigeru Hashimoto and Masaaki Murakami
N15 W7, Kita-ku, Sapporo, Hokkaido 060-8638, Japan
e-mail: hashimot@igm.hokudai.ac.jp and murakami@igm.hokudai.ac.jp

Satoshi Yamada
1-1 Ridai-cho, Okayama 700-0005, Japan.
e-mail: yamada@are.ous.ac.jp

Keywords:
Computer modeling, Cytokine, Arthritis model, IL-6, IL-17

Abstract

The IL-6 amplifier, which describes the simultaneous activation of STAT3 and NF-kB, in synovial fibroblasts causes the infiltration of immune cells into the joints of F759 mice. The result is a disease that resembles human rheumatoid arthritis. However, the kinetics and regulatory mechanisms of how augmented transcriptional activation by STAT3 and NF-kB leads to F759 arthritis is unknown. We here show that the STAT3-NF-kB complex is present in the cytoplasm and nucleus and accumulates around NFkB binding sites of the IL-6 promoter region and established a computer model that shows IL-6 and IL-17 signaling promotes formation of the STAT3-NF-kB complex followed by its binding on promoter regions of NF-kB target genes to accelerate inflammatory responses, including the production of IL-6, epiregulin, and CCL2, phenotypes consistent with *in vitro* experiments. The binding also promoted cell growth in the synovium and the recruitment of Th17 cells and macrophages in the joints. Anti-IL-6 blocking antibody treatment inhibited inflammatory responses even at the late phase, but anti-IL-17 and anti-TNFα antibodies did not. However, anti-IL-17 antibody at the early phase showed inhibitory effects, suggesting that the IL-6 amplifier is dependent on IL-6 and IL-17 stimulation at the early phase, but only on IL-6 at the late phase. These findings demonstrate the molecular mechanism of F759 arthritis can be recapitulated *in silico* and identify a possible therapeutic strategy for IL-6 amplifier-dependent chronic inflammatory diseases.

Introduction

Rheumatoid arthritis (RA) is a common autoimmune disease characterized by chronic inflammation in the joints [1]. Inflammatory cytokines including interleukin-6 (IL-6) play a role in RA, and an anti-IL-6-receptor (IL-6R) antibody, tocilizumab, shows outstanding effects [2]. To investigate the molecular mechanism of the disease, we established mutant mice (F759 mice) that have a point mutation that changes tyrosine residue 759 in gp130, an IL-6 signal transducer in the IL-6 receptor complex, into a phenylalanine residue [3]. Because phosphorylated tyrosine 759 is the binding site of SOCS3, which induces a negative feedback loop for IL-6 signaling [2], IL-6-mediated STAT3 activation is enhanced in F759 mice to spontaneously develop an RA-like disease (F759 arthritis) with age [3,4]. Using F759 mice, we discovered the IL-6 amplifier, which is a mechanism for tissue-specific inflammation and enhanced NF-κB activation in non-immune cells, including synovial fibroblasts and endothelial cells. Activation of the IL-6 amplifier causes the expression of inflammation mediators, including chemokines and growth factors, in animal models and RA patients [5,6]. Further, we showed that an enhanced IL-6 signal in type 1 collagen+ (Col1a)+ non-immune cells is responsible for the development of F759 arthritis. F759 arthritis was developed even in RAG-deficient F759 mice upon IL-6 plus IL-17 injections in the joints [4], even though F759 arthritis is dependent on Th17 cell accumulation in the joints [5], indicating that Th17 cells in the joints are cytokine producers that promote inflammation via the IL-6 amplifier. In fact, direct ankle-joint injections of cytokines in young F759 mice caused an arthritic disease within two weeks [7-9]. Moreover, epiregulin, which is a growth factor and a ligand of ErbB1, is induced at the earliest stage of IL-6 amplifier activation and followed by the enhanced expression of chemokines including CCL20 and other growth factors to accumulate immune cells via NF-kB activation in F759 arthritis [7,9]. We have investigated the role of the IL-6 amplifier in various mouse disease models, including osteoarthritis, multiple sclerosis, psoriasis, uveoretinitis, and chronic rejection, and in human samples of numerous patients affected by the same and other inflammatory diseases [5, 7-25]. This investigation led us to conclude that IL-6 is the most common cytokine that activates STAT3 during inflammatory diseases and that different cell types have their own triggers for the IL-6 amplifier [2].

Several computer techniques have been applied to the study of RA. Artificial intelligence, in particular deep learning models, has been used in clinical studies to support diagnosis from X-ray images [26] and the prediction of clinical outcomes [27]. Additionally, a computer simulation was done to study cytokine-induced cartilage breakdown [28]. However, computer models using data from RA patients and/or animal models are not reported.

In this study, we developed a computer model of F759 arthritis to show the minimum factors for arthritis development in the presence of the STAT3-NF-kB complex. The model compared cytokine simulations in non-immune cells from wild-type and F759 mice and recapitulated the concentration dependency on IL-6 and IL-17 in the IL-6 production and the time course of the nuclear translocation of the STAT3-NF-kB complex *in vitro*. Simulations of the spontaneous onset of F759 arthritis demonstrated that the promoter activity of NF-kB and the expression of epiregulin were increased by the IL-6 amplifier. Finally, antibody treatments against inflammatory

cytokines *in silico* revealed that F759 arthritis development is dependent on IL-6 and IL-17 in the early stages of the disease but only on IL-6 in the late stages.

Material and methods

Cell lines and stimulation conditions

Immortalized synovial fibroblasts were plated in 96-well plates (1×10^4 cells/well) and stimulated with human IL-6 (100 ng/mL; Toray Industries, Tokyo, Japan) plus human soluble IL-6 receptor (100 ng/mL; R&D Systems, Tokyo) and mouse IL-17A (50 ng/mL; R&D Systems) as well as TNFα (50 ng/mL; PEPROTECH) for the indicated periods after serum starvation for 2 hrs. The addition of soluble IL-6 receptor is required for the stimulation of cells with no or low expression of the IL-6 receptor chain such as non-immune cells including fibroblasts and endothelial cells. Mouse cells are responsive to human IL-6, which allowed us to measure mouse IL-6 in the culture supernatant using mouse-specific IL-6 ELISA (eBioscience and BD Biosciences). Cell culture supernatant was collected for ELISA, and cell growth was assessed by the MTT assay. Cells were harvested, and total RNA was prepared for real-time PCR.

ChIP Assay

Immortalized wild-type or F759 fibroblasts were stimulated with IL-6 and IL-17 from 0 to 50 hours. Cells were fixed with 1% PFA and lysed with lysis buffer (10 mM Tris-HCl [pH 7.5], 140 mM NaCl, 1% TX-100, 1 mM EDTA, and 1% SDS). The lysate was sonicated to prepare chromatin DNA. Immunoprecipitation was performed with Dynabeads protein G (Life Technologies, Tokyo), and phospho-STAT3 antibody (Cell Signaling Technology) was added. DNA purification was done with 10% Chelex100 (40 μL; BIO-RAD, Tokyo). Real-time PCR was performed with IL-6 promoter primer pairs that included a NF-kB binding site.

Cell fractionation

Nuclear/cytosolic fractionation was carried out following the manufacturer's protocol (AKR-171, CELL BIOLABS). Briefly, HEK293T cells were transfected with pEFBOS-HA-p65 or pEFBOS empty plasmids and pEFBOS-human STAT3-Flag with polyethyleneimine. After 24 hours, the cells were starved with Opti-MEM Reduced Serum Medium (Gibco) for 3 hours, stimulated for 30 min with 100 ng/mL human IL-6 (Toray Industries) plus 100 ng/mL soluble IL-6R (R&D Systems) and 50 ng/mL TNF-α (PeproTech), and then 5 x 10^6 cells were collected by centrifugation for 5 min at 4°C (x 600 g). The cell pellet was resuspended with 500 μL of ice-cold Cytosol Extraction Buffer containing DTT/Protease Inhibitors. After incubation on ice for 10 min, the cells were lysed in 25 μL of Cell Lysis Reagent and vortexed for 10 s at the highest setting, followed by centrifugation for 10 min at 4°C (800 *g*). The supernatant (cytoplasmic fraction) was carefully transferred to a clean, chilled microcentrifuge tube and stored at 80°C. The wash step was repeated to reduce cross-contamination between fractions. The nuclear pellet was gently resuspended with 100 μL of Nuclear Extraction Buffer containing DTT/Protease Inhibitors, maintained on ice for 30 min, vortexed for 10 s at the highest setting at 10 min intervals, and centrifuged for 30 min at 4°C (14,000 *g*). The supernatant (nuclear fraction) was transferred to a clean, chilled microcentrifuge tube and stored at 80°C. Both the nuclear and cytosolic fractionated solutions were dialyzed and concentrated using Ultrafiltration spin columns (SR-3510 and PT-1001, APRO Science) for exchange to Buffer-B (20 mM Tris [pH 7.8], 100 mM KCl, 10% glycerol,

0.2% Triton X-100, 0.5 mM PMSF, and 1 μg each of leupeptin, antipain, pepstatin, and chymostatin per mL).

Immunoprecipitation Analysis

After quickly washing with PBS on ice, the cells were collected by scraping and then lysed in Buffer-B at 4°C for 30 min. After clarifying by centrifugation, 300 μg of the cell lysates was precleared with 30 μL of protein G-sepharose (Pharmacia) for 30 min and incubated with 30 μL of FLAG beads (Sigma-Aldrich) at 4°C for 2 hours. After washing with Buffer-B three times, the beads were resuspended in Laemmli buffer and boiled for 3 min, and the eluted proteins were used for western blotting.

Assay for transposase accessible chromatin using sequencing (ATAC-seq)

ATAC-seq was performed using the ATAC-Seq Kit (53150, Active Motif). Briefly, 1 x 10^5 immortalized fibroblasts derived from wild-type and F759 mutant C57BL/6 mice were used to isolate nuclei. Nuclei were incubated with Tagmentation Master Mix at 37°C for 30 minutes after lysing the cells in ice-cold ATAC Lysis Buffer in the kit, and the DNA was purified with a DNA purification column. PCR amplification of tagmented DNA was performed to make libraries with the appropriate indexed primers. After SPRI bead clean-up, the DNA libraries were analyzed to assess the size distribution with a Bioanalyzer 2100 (Agilent) and then sequenced on a DNBSEQ (MGI) (100 bp PE, 800 million reads) at the Kazusa DNA Institute (Chiba, Japan).

ATAC-seq data analysis

Quality control of the ATAC-seq reads was carried out using fastqc (v.0.11.9), fastp (v.0.22.0) and picard (v.0.1.2). The reads were then mapped to reference the mouse genome (mm10, https://genome-idx.s3.amazonaws.com/bt/mm10.zip) with bowtie2 (v.2.2.5). Peak calling was performed using MACS3 (v.3.0.0a7). Integrative Genomics Viewer (IGV, v.2.16.0) was used to visualize the genomic data, and ChIP-Atlas (https://chip-atlas.org/) was applied to view the p65 and STAT3 binding regions on the given genomic loci with the IGV genome browser.

Statistical analysis

Student's t-tests (two-tailed) were used for the statistical analysis of differences between two groups. P values less than 0.05 were considered statistically significant.

Results

STAT3 and NF-kB are associated in the cytoplasm and nucleus

To investigate how the NF-kB pathway is enhanced in the presence of IL-6-STAT3 during activation of the IL-6 amplifier, we analyzed the association of STAT3 and NF-kB in nonimmune cells (293T cells). We forced the expression of STAT3 or NF-kB and fractionated proteins in the cytoplasm and nucleus. We found STAT3 and NF-kB were associated in both cellular regions, although more so in the nucleus (Fig. 1A). Our ATAC-seq after IL-6 amplifier activation and ChIP-seq experiments suggested that the STAT3-NF-kB complex is present on open chromatin regions with RNA polymerase II accumulation in the promoter regions of some NF-kB targets, including IL-6, which did not show obvious STAT3 binding sites (Fig. 1B-1D). These results strongly suggest that the STAT3-NF-kB complex plays an important role in the activation of the IL-6 amplifier and subsequent development of F759 arthritis. Therefore, it is reasonable that the STAT3-NFkB complex enhances NF-kB promoter activity.

Establishment of a computational model for F759 arthritis

We established a computer model with the STAT3-NFkB complex as the only transcription factor for target genes of the IL-6 amplifier.

Figure 2A shows the intracellular kinetics scheme of the IL-6 amplifier signaling network in synovial fibroblasts. STAT3 activation includes the binding of IL-6 to its receptor to phosphorylate Janus kinase (JAK) and STAT3 in the cytoplasm. Phosphorylated STAT3 moves to the nucleus after complexing with phosphorylated NF-kB to bind to the NF-kB binding site to produce IL-6, epiregulin, and chemokines. Because F759 mice have a point mutation in gp130, SOCS3 fails to function as a negative regulator. IL-17-, TNFα-, and epiregulin-mediated NF-kB activation positively regulate phosphorylation of the IkB kinase (IKK) complex. The activated IKK complex together with BCR-CK2 (not shown) leads to the phosphorylation of IkB and NF-kB [8]. The resulting dissociation of NF-kB and IkB allows phosphorylated NF-kB and phosphorylated STAT3 to enter the nucleus as a complex. This complex binds to NF-kB target genes to produce IL-6, chemokines, and growth factors, including CCL20, CCL2, and epiregulin.

To mimic the development of RA, a computational model of the joint was made (Fig. 2B). Th17 cells and macrophages infiltrate from the blood to the joint in response to microbleeding, and CCL2 and CCL20 signaling enhances the infiltration. Th17 cells produce IL-17, while macrophages produce IL-6 and TNFα.

All reactions are represented as mass-action kinetics. Two hierarchical structures in this computational model were simulated, a cell and a joint, which were divided into two compartments, respectively, the cytoplasm and nucleus and the blood and joint. The model assumes the active STAT3-NF-kB complex enters the nucleus, and it includes proteins of functional NF-kB target genes, such as *IL-6*, *CCL2*, *CCL20*, and *epiregulin*. Parameter values and initial concentrations for the STAT3-activating pathway were based on our previous simulations of the IFN-γ signaling pathway [29] and Th0 cell differentiation [30]. Parameter values and initial concentrations for the NF-kB activating pathway were based on the JAK/STAT signaling pathway but modified such that the time courses of the NF-kB activation and STAT3 activation were similar. Parameters for the internalization of IL-6 receptors were based on EGF receptors [31]. The translation rate of mRNA was proportional to the concentration of the STAT3-NF-

kB complex. The transcription rate depended on the concentration of active transcription factors but had a plateau due to the limited number of RNA polymerase complexes. The Michaelis-Menten equation was not used because the substrate concentration is rarely much larger than the concentration of the enzyme.

Thus, the phosphorylation of NF-kB by IKKP is described by the following chemical reactions:
[NF-kB]+[IKKP]<->[NF-kB-IKKP], [NF-kB-IKKP]->[NF-kBP-IKKP], [NF-kBP]+[IKKP]<->[NF-kBP-IKKP].

The chemical reaction of [IL6]+[IL6R]<->[IL6-IL6R] is described as $\frac{d[IL6-IL6R]}{dt} = k_1[IL6][IL6R] - k_{-1}[IL6 - IL6R]$ and $\frac{d[IL6]}{dt} = -k_1[IL6][IL6R] + k_{-1}[IL6 - IL6R]$.

All chemical reactions are described by differential equations and presented in Table 1. The differential equations were solved mathematically using the Runge-Kutta-Gill method.

Concentration dependency of IL-6 levels on IL-6 and IL-17 in silico and in vitro.

To investigate whether the activation pattern and intensity of the IL-6 amplifier are similar between wild-type and F759 mice *in silico* and *in vitro*, we compared the concentration dependency of IL-6 levels on IL-6 and IL-17 *in silico* and *in vitro*. We found the dependency of *IL-6* expression on the concentrations of IL-6 and IL-17 in synovial fibroblasts derived from wild-type and F759 mice was similar *in silico* and *in vitro* (Fig. 3A and 3B). The culture system used made it difficult to reduce the background level of IL-6 expression, because the stimulatory signaling by low FCS, which is critical for cell survival, in starvation medium increased NF-kB and STAT3 signaling. This increased signaling increased IL-6 mRNA levels in the presence of either IL-6 or IL-17. Furthermore, we previously demonstrated that growth factors directly activated the IL-6 amplifier to develop some inflammatory diseases [7,9]. Therefore, although *in vitro* experiments with 0 nM of each cytokine expressed low levels of IL-6, we hypothesized the low levels were because of growth factors in FCS that stimulated the NF-kB (Fig. 3B).

Time courses of the activation status of STAT3 and NF-kB and IL-6 expression after IL-6 amplifier activation.

We next compared simulated time courses of the nuclear localization of activated STAT3 and NF-kB and IL-6 levels in wild-type and F759 fibroblasts with experimental data. IL-6 and IL-17 *in silico* induced the translocalization of STAT3 and NF-kB into the nucleus of synovial fibroblasts and the expression of IL-6 in the initial 10 to 20 hours (Fig. 4A and 4C). In wild-type synovial fibroblasts, the complex level in the nucleus and IL-6 expression were decreased in the presence of SOCS3-mediated negative regulation of STAT3 phosphorylation. On the contrary, in F759 synovial fibroblasts, both the STAT3-NF-kB complex and IL-6 levels were augmented (Fig. 4A and 4C). Similar phenomena were observed *in vitro* (Fig. 4B and 4D): IL-6 and IL-17 stimulation induced the translocalization of STAT3 into the nucleus of synovial fibroblasts and NF-kB-mediated IL-6 expression in the initial 10 to 15 hours; in wild-

type synovial fibroblasts, the complex formation in the nucleus and IL-6 expression decreased due to the tyrosine phosphorylation of STAT3 by SOCS3, but in F759 synovial fibroblasts, both the STAT3-NF-kB complex and IL-6 levels were maintained for at least 50 to 70 hours after stimulation. The culture system we used makes it difficult to conduct *in vitro* experiments at longer time points because cell proliferation by low FCS in starvation medium gradually increases the number of cells to induce growth arrest and decreases the amount of cytokines treated in the limited area of culture equipment. We hypothesize that the growth arrest and reduction of cytokines are responsible for the different tendencies, particularly at the later time points, compared to the simulation results.

IL-6 and IL-17 stimulation induces IL-6 in nonimmune cells depending on Th17 cells in the blood in silico.

In the computer model, the STAT3-NF-kB complex but not NF-kB alone has transcriptional activity. Consistently, IL-6 expression in nonimmune cells was dependent on the IL-6 amplifier, which is activated by the STAT3-NF-kB complex via IL-6 and IL-17 stimulation (Fig. 5A), whereas removing the STAT3-NF-kB complex from the model disrupted the relationship between IL-6 expression and IL-6 and IL-17 concentrations (Fig. 5B).

IL-17 is mainly produced by Th17 cells [4,6], while macrophages produce more IL-6 as well as TNFα. We previously found that Th17 cells and macrophages are increased in the blood of F759 mice with age [3], suggesting they are key regulatory cells of F759 arthritis. We therefore simulated the effects of different concentrations of Th17 cells and macrophages in the blood on the expression levels of *IL-6*. *IL-6* expression in nonimmune cells of the joints showed a positive relationship with Th17 cells and macrophages in the presence of the STAT3-NF-kB complex (Fig. 6A and 6B).

Production of cytokines and chemokines and infiltration of Th17 cells and macrophages in the joints in silico.

The binding of cytokines, such as IL-6, IL-17, and TNFα, to their receptors induces receptor phosphorylation and transcription factor activation. STAT3 and NF-kB are activated mainly by IL-6-STAT3 and NF-kB stimulators, including IL-17 and TNFα, to simultaneously translocate to the nucleus after the complex formation, where they act as transcription factors for several NF-kB-target genes including *epiregulin*, *IL-6*, *CCL2*, and *CCL20*. Indeed, epiregulin, which is a growth factor, is induced at the earliest stage of IL-6 amplifier activation and before the enhanced expression of other inflammatory factors in F759 arthritis [7], although IL-6 maintains STAT3 activation and chemokines accumulate immune cells from the blood [2]. The model revealed that in wild-type mice, the presence of SCOS3 negatively regulated *epiregulin*, *IL-6*, *CCL2*, and *CCL20* in the joints (Fig. 7A), indicating that the disease development is dependent on the IL-6-STAT3 pathway.

Because F759 arthritis was developed after six months in F759 mice, the *in silico* model was designed with a similar time course. Because SOCS3 is inactive in F759 mice, the nuclear localization of activated STAT3 was increased by around day 70 and sustained (Fig. 7B). Nuclear NF-kB was augmented from around day 100 and sustained. The active STAT3-NF-kB complex was increased at around day 120 and sustained, and the expression levels of *epiregulin*, *IL-6*, *IL-17*, and *CCL2* in the joint

and SOCS3 in the synovial fibroblasts were increased thereafter (Fig. 7B), although there is no SOCS3 binding site in gp130. Moreover, in the joint, the infiltration of Th17 cells and macrophages was enhanced at around day 120 (Fig. 7B). Additionally, the concentration of epiregulin was sufficient to proliferate synovial fibroblasts and to sustain the activation of the IL-6 amplifier. These findings indicate that IL-6 amplifier activation in the joints is critical for the induction of F759 arthritis.

Effects of antibodies against cytokines in silico.

We then investigated *in silico* the effects of antibody treatments against inflammatory cytokines such as IL-6, TNFα, and IL-17 on the production of cytokines and chemokines and the accumulation of Th17 cells and macrophages in the joints of F759 mice. The simulated administration of anti-IL-6 antibody at day 250 inhibited STAT3 activation, activated NF-kB, and promoted STAT3-NF-kB complex formation as well as CCL2, SOCS3, and epiregulin production compared with untreated F759 mice (Fig. 8A and 8B), findings consistent with the clinical effects of the anti-IL-6 and /or anti-IL-6R blocking antibodies sirukumab and tocilizumab [32]. Additionally, the expression of epiregulin was decreased at day 300 (Fig. 8F).

Although anti-TNFα antibodies, such as infliximab and adalimumab, are also clinically used to treat RA patients [32], the simulated treatment with anti-TNFα antibodies at day 250 did not suppress NF-kB- and STAT3-mediated inflammatory responses (Fig. 8C). Neither did the simulated administration of anti-IL-17 antibody or anti-TNFα and anti-IL-17 antibody combination (Fig. 8D and 8E). Consistently, the expression of epiregulin was not decreased at day 300 (Fig. 8F). These results suggest that there are several molecular mechanisms of RA and this simulation represents one subtype of RA. Moreover, anti-IL-17 antibody treatment at day 50 but not day 100 inhibited almost all factors related to the IL-6 amplifier (Fig. 8G and 8H). Anti-IL-6 antibody but not anti-TNFα antibody treatment at day 50 also suppressed F759 arthritis development (Fig. S1). These simulation results strongly suggest that IL-6 plays an important role in the F759 arthritis pathogenesis in the early and late stages, but with IL-17 from Th17 cells playing an important role only in the early stage. Consistent with the IL-17 observations, we previously showed that IL-17A deficient-F759 mice have suppressed F759 arthritis development [6].

Sensitivity analysis in silico.

Finally, to identify the crucial factors in F759 arthritis development, we performed a sensitivity analysis [33], in which we varied the relative value of individual kinetics parameters from 1/10 to 10 and examined the epiregulin production. Sensitivity was defined as the slope of the epiregulin production on the parameter dependency (dashed lines in Fig. 9A), and the sensitivities are shown in Fig. 9B. Large sensitivities were defined as sensitivities $\geq|5|$ and found for parameters in the NF-kB-activating pathway (a, b, c, d), in the STAT3-activating pathway (o, p), in STAT3-NF-kB complex binding (e), in the migration of Th17 cells (t, u), in IL-17 production by Th17 cells (q), in the proliferation of synovial fibroblasts (n), and in the migration of macrophages (v, w). Consistent with *in vitro* and *in vivo* studies on the development of F759 arthritis [7, 9,34], these results suggest that multiple factors are involved in the augmentation of epiregulin production to cause F759 arthritis. Thus, molecular events in these reactions

may be promising targets for the development of novel diagnostic and therapeutic approaches for IL-6 amplifier-associated inflammatory diseases.

Discussion

We here established a computer model for the development of F759 arthritis. This is the first computer simulation of the development of RA in animal models. Because we showed that the STAT3-NF-kB complex forms in the cytoplasm and nucleus, a feature that may be necessary for the activation of the IL-6 amplifier, we assigned the STAT3-NF-kB complex, but not NF-kB alone, to have transcriptional activity in our model. Moreover, because we previously showed that epiregulin, which is a growth factor and NF-kB stimulator, was induced at the earliest stage of the amplifier activation [7,9], we focused on its expression in the joints as a regulator of F759 arthritis. Our computer model demonstrated that the STAT3-stimulating factor is IL-6 from the early to late stages of the pathogenesis and that the NF-kB-stimulating factor of the IL-6 amplifier changes from IL-17A derived from Th17 cells to epiregulin derived from synovial cells. Thus, our computer model of F759 arthritis may represent a type of pathogenesis of IL-6-dependent RA development, because some therapeutic agents, such as anti-IL-6R antibody but not anti-TNFα antibody are effective in some RA patient subgroups [32, 35].

RA is a devastating autoimmune disease characterized by persistent synovial inflammation leading to joint destruction. The pathogenesis of RA is based on the dysregulation of a variety of molecules in immune cells (T cells, B cells, monocytes, etc.) and non-immune cells against a background of genetic predispositions and environmental factors. Synovial fibroblasts are multifunctional mesenchymal cells that reside in the perisynovial surface layer. In RA, synovial fibroblasts are involved in the induction and persistence of synovitis through the high expression of proinflammatory cytokines such as IL-6. Recently developed biologics and molecular-targeted drugs have greatly advanced the treatment of RA by directly inhibiting inflammatory cytokines, co-stimulatory molecules between T cells and antigen-presenting cells, and their signaling pathways [32]. However, the inadequate efficacy of these agents in some patients and severe side effects due to systemic immunosuppression caused by their administration remain a major challenge [36]. Therapeutic developments targeting synovial fibroblasts, which play a central role in the formation of synovitis at the joint site, have the potential to overcome these challenges.

The F759 mutation prevents SOCS3 from interacting with gp130, thus enhancing JAK-dependent STAT3 activation by IL-6 to spontaneously develop an RA-like arthritic disease with age in mice [3]. Importantly, the F759 mutation causes the pathology to begin in non-immune cells in the presence of Th17 cells in the blood [4-6]. Furthermore, an analysis using F759 mice revealed that the IL-6 amplifier is activated by the joint accumulation of Th17 cells from the blood [4,6].

In this study, we established a computer model that showed IL-6 amplifier activation in synovial fibroblasts plays an important role in the pathogenesis of F759 arthritis. We first showed the direct association between STAT3 and NF-kB in the cytoplasm and nucleus. ATAC-seq experiments showed that the promoter regions of IL-6, CCL2, epiregulin, in which NF-kB, STAT3, and RNA polymerase II were accumulated, were opened after activation of the IL-6 amplifier in F759 fibroblasts.

A comparison of IL-6 amplifier activation in fibroblasts isolated from wild-type and F759 mice found a concentration dependency on IL-6 and IL-17 for *IL-6* expression *in silico* and *in vitro*. We then examined the spontaneous onset of F759 arthritis and found the triggering factor is the accumulation of blood Th17 cells

expressing IL-17 and IL-6 migrating to the joints. The cytokine simulation reproduced the nuclear translocation of activated STAT3-NF-kB complex in synovial fibroblasts, the increased production of epiregulin and cytokines including IL-6, and the infiltration of macrophages and Th17 cells in the joints of F759 mice over time and the succeeding increase in TNFα, IL-17, and epiregulin levels. The effects of cytokine-blocking antibodies on the production of cytokines and the infiltration of Th17 cells and macrophages into the joints indicated that the pathogenesis of F759 arthritis is mediated by the IL-6 amplifier in synovial cells. The antibody effects also indicated that IL-6 plays essential roles in the early and late stages of the disease, but IL-17 plays an essential role only in the early phase. Finally, to identify important responses in the pathogenesis, we performed a sensitivity analysis on epiregulin production and found significant changes in several parameters that fall into five major categories (Fig. 9). Elucidating the molecular basis associated with these parameters may provide promising targets for the development of novel diagnostic and therapeutic approaches for IL-6-amplifier-associated inflammatory diseases including RA.

Epiregulin is a growth factor and a ligand for ErbB1, which contributes to inflammatory diseases via the IL-6 amplifier [7,9]. In fact, serum epiregulin is elevated in patients with RA, atherosclerosis, and multiple sclerosis [7,9]. Moreover, GWAS comparisons confirmed an association between these diseases and genes related to the IL-6 amplifier, and in the absence of epiregulin, IL-6 expression was significantly decreased even after activation of the IL-6 amplifier [7]. Epiregulin plays an important role in NF-kB activation via the PI3K pathway. Since epiregulin is a target of the IL-6 amplifier and affects various steps of inflammation, the amount of epiregulin should reflect the activity of the IL-6 amplifier *in vivo*. Therefore, in this study, epiregulin was chosen as the parameter to represent the onset of inflammation and the development of F759 arthritis. Our computer model showed that in F759, epiregulin was produced from a relatively early phase (Fig. 7). It also revealed that anti-IL-17 antibodies suppressed epiregulin expression and inflammation when administered early but not late (Fig. 8D and 8G), whereas anti-IL-6 antibody suppressed epiregulin at both phases (Fig. 8B and Fig. S1A). These data suggest that IL-6 and IL-17 initiate IL-6 amplifier activation and gradually increase epiregulin production in the early phase and that IL-6 and epiregulin are involved in maintaining inflammation during the late phase. Clinically, RA patients often suffer osteoporotic fractures. With regard to osteoporosis, epiregulin is considered a key factor that activates osteoclasts via EGFR signaling and stimulates the RANKL-mediated osteoclastogenic signaling pathway [37]. Therefore, controlling the production of epiregulin may reduce the aggravation of RA, and factors in the molecular mechanism for epiregulin production by the IL-6 amplifier may provide excellent targets for the development of new drugs.

TNFα, a NF-kB stimulator, is one of the most notable inflammatory cytokines in RA arthritis. Several drugs target it including adalimumab. Although the efficacy of anti-TNFα antibodies do not match that of anti-IL-6 antibodies in some RA patients, combination therapy with methotrexate has been clinically effective. However, in our computer model, the suppressive effect of anti-TNFα antibodies on IL-6, IL-17, epiregulin, and other factors was almost negligible (Fig. 8C and Fig. S1B). There are two probably reasons for this result. First, values of the kinetics parameters for TNFα production by macrophages were smaller than for the production of IL-17, another NF-kB stimulator, by Th17 cells, meaning that TNFα-mediated NF-kB activation was

relatively smaller than IL-17-mediated activation in our model. Second, focusing only on pathways strongly associated with the IL-6 amplifier may have resulted in some pathways responsible for TNFα production by CD4+ T cells, other immune cells, etc., which are not reflected well in our model. The mechanism of action of anti-TNFα antibodies has been noted to involve the suppression of multiple inflammatory cytokines, the reduction of immune cell infiltration, the interference of osteoclast activation, and the reduction of angiogenesis [38]. Thus, other TNFα effects should be included in the model to study the clinical effects of these antibodies. Moreover, because several RA patients are less responsive to anti-TNFα antibodies than to anti-IL-6R antibodies [2], the model in its current form may reflect the pathophysiology of this patient subgroup.

In conclusion, we established a novel *in silico* model of F759 arthritis and used it investigate the IL-6 amplifier in the joints, including the molecular mechanism of its activation and the effects of antibodies. We showed that IL-6 amplifier activation with the sustained expression of epiregulin in non-immune cells leads to the development of F759 arthritis. Integrating more pathways into this model will accelerate our understanding of the pathogenesis of RA and lead to the creation of novel strategies for RA therapeutics.

Table 1. Differential equations for biochemical reactions and kinetic parameters

Pathway	No.	differential equations	parameters
NFkB activating pathway	**A-1**	$\frac{d[IKKP]c}{dt} = k_f \frac{[IL-17]j}{K_m + [IL-17]j}$	k_f=5x 10^{10} K_m=5nM
	A-2	$\frac{d[IKKP]c}{dt} = k_f \frac{[TNF]j}{K_m + [TNF]j}$	k_f=5x 10^{10} K_m=5nM
	A-3	$\frac{d[IKKP]c}{dt} = k_f \frac{[epiregulin]j}{K_m + [epiregulin]j}$	k_f=5x 10^{10} K_m=5nM
	A-4	$\frac{d[NFkB\_IkBa]c}{dt} - k_1[NFkB]c[IkBa]c - k_{-1}[NFkB\_IkBa]c$ $\frac{d[NFkB]c}{dt} - -k_1[NFkB]c[IkBa]c + k_{-1}[NFkB\_IkBa]c$ $\frac{d[ikBa]c}{dt} - -k_1[NFkB]c[IkBa]c + k_{-1}[NFkB\_IkBa]c$	k_1=5x 10^8 k_{-1}=0.025 K_d=0.05nM
	A-5	$\frac{d[NFkBP\_IkBa]c}{dt} - k_1[NFkBP]c[IkBa]c - k_{-1}[NFkBP\_IkBa]c$ $\frac{d[NFkBP]c}{dt} - -k_1[NFkBP]c[IkBa]c + k_{-1}[NFkBP\_IkBa]c$ $\frac{d[ikBa]c}{dt} - -k_2[NFkBP]c[IkBa]c + k_{-1}[NFkBP\_IkBa]c$	k_1=5x 10^7 k_{-1}=0.05 K_d=1nM
	A-6	$\frac{d[ikBa\_IKKP]c}{dt} - k_1[IkBa]c[IKKP]c - k_{-1}[IkBa\_IKKP]c$ $\frac{d[ikBa]c}{dt} - -k_1[IkBa]c[IKKP]c + k_{-1}[IkBa\_IKKP]c$ $\frac{d[IKKP]c}{dt} - -k_1[IkBa]c[IKKP]c + k_{-1}[IkBa\_IKKP]c$	k_1=5x 10^7 k_{-1}=0.05 K_d=1nM
	A-7	$\frac{d[IkBaP\_IKKP]c}{dt} - r_p[IkBa\_IKKP]c$ $\frac{d[IkBa\_IKKP]c}{dt} - -r_p[IkBa\_IKKP]c$	r_p=0.05
	A-8	$\frac{d[IkBaP\_IKKP]c}{dt} - k_1[IkBaP]c[IKKP]c - k_{-1}[IkBaP\_IKKP]c$ $\frac{d[ikBaP]c}{dt} - -k_1[IkBaP]c[IKKP]c + k_{-1}[IkBaP\_IKKP]c$ $\frac{d[IKKP]c}{dt} - -k_1[IkBaP]c[IKKP]c + k_{-1}[IkBaP\_IKKP]c$	k_1=10^7 k_{-1}=0.2 K_d=20nM
	A-9	$\frac{d[NFkB\_IKKP]c}{dt} - k_1[NFkB]c[IKKP]c + k_{-1}[NFkB\_IKKP]c$ $\frac{d[NFkB]c}{dt} - -k_1[NFkB]c[IKKP]c + k_{-1}[NFkB\_IKKP]c$ $\frac{d[IKKP]c}{dt} - -k_1[NFkB]c[IKKP]c + k_{-1}[NFkB\_IKKP]c$	k_1=5x 10^7 k_{-1}=0.05 K_d=1nM
	A-10	$\frac{d[NFkBP\_IKKP]c}{dt} - r_p[NFkB\_IKKP]c$ $\frac{d[NFkB\_IKKP]c}{dt} - -r_p[NFkB\_IKKP]c$	r_p=0.005
	A-11	$\frac{d[NFkBP\_IKKP]c}{dt} - k_1[NFkBP]c[IKKP]c - k_{-1}[NFkBP\_IKKP]c$ $\frac{d[NFkBP]c}{dt} - -k_1[NFkBP]c[IKKP]c + k_{-1}[NFkBP\_IKKP]c$ $\frac{d[IKKP]c}{dt} - -k_2[NFkBP]c[IKKP]c + k_{-1}[NFkBP\_IKKP]c$	k_1=10^7 k_{-1}=0.2 K_d=20nM
	A-12	$\frac{d[NFkB]c}{dt} - r_d[NFkBP]c$ $\frac{d[NFkBP]c}{dt} - -r_d[NFkBP]c$	r_d=0.002
	A-13	$\frac{d[NFkBP]n}{dt} = r_m[NFkBP]c$ $\frac{d[NFkBP]c}{dt} - r_m[NFkBP]c$	r_m=0.002
	A-14	$\frac{d[NFkBP]c}{dt} - r_m[NFkBP]n$ $\frac{d[NFkBP]n}{dt} - r_m[NFkBP]n$	r_m=0.001
	A-15	$\frac{d[IkBa]n}{dt} - k_f \frac{[NFkBP]n}{K_t + [NFkBP]n}$	k_f=2x 10^8 K_t=2nM
	A-16	$\frac{d[ikBa]c}{dt} - r_m[IkBa]n$ $\frac{d[IkBa]n}{dt} = -r_m[IkBa]n$	r_m=0.01

Table 1. (*Continued*)

STAT3 activating pathway	**B-1**	$\frac{d[IL6 \quad IL6R]c}{dt} - k_1[IL6]j[IL6R]c - k_{-1}[IL6 - IL6R]c$ $\frac{d[IL6]j}{dt} - (-k_1[IL6]j[IL6R]c + k_{-1}[IL6 - IL6R]c)\frac{1}{\tau}$ $\frac{d[IL6R]c}{dt} - -k_1[IL6]j[IL6R]c + k_{-1}[IL6 - IL6R]c$	k_1=2x10^8	k_{-1}=0.02	K_d=10nM	r=30
	B-2	$\frac{d[IL6R \quad JAK]c}{dt} - k_1[IL6R]c[JAK]c - k_{-1}[IL6R - JAK]c$ $\frac{d[IL6R]c}{dt} - -k_1[IL6R]c[JAK]c + k_{-1}[IL6R - JAK]c$ $\frac{d[JAK]c}{dt} - -k_1[IL6R]c[JAK]c + k_{-1}[IL6R - JAK]c$	k_1=10^8	k_{-1}=0.05	K_d=0.5nM	
	B-3	$\frac{d[IL6 \quad IL6R \quad JAK]c}{dt} - k_1[IL6 - IL6R]c[JAK]c - k_{-1}[IL6 - IL6R - JAK]c$ $\frac{d[IL6 \quad IL6R]c}{dt} - -k_1[IL6 - IL6R]c[JAK]c + k_{-1}[IL6 - IL6R - JAK]c$ $\frac{d[JAK]c}{dt} - -k_1[IL6 \quad IL6R]c[JAK]c + k_{-1}[IL6 \quad IL6R \quad JAK]c$	k_1=10^8	k_{-1}=0.05,	K_d=0.5nM	
	B-4	$\frac{d[IL6 \quad IL6R \quad JAK]c}{dt} - k_1[IL6]j[IL6R - JAK]c - k_{-1}[IL6 - IL6R - JAK]c$ $\frac{d[IL6]j}{dt} - (-k_1[IL6]j[IL6R - JAK]c + k_{-1}[IL6 - IL6R - JAK]c)\frac{1}{\tau}$ $\frac{d[IL6R \quad JAK]c}{dt} - -k_1[IL6]j[IL6R - JAK]c + k_{-1}[IL6 - IL6R - JAK]c$	k_1=2x10^8	k_{-1}=0.02	K_d=10nM	r=30
	B-5	$\frac{d[IL6 \quad IL6R \quad JAKP]c}{dt} - r_p[IL6 - IL6R - JAK]c$ $\frac{d[IL6 \quad IL6R \quad JAK]c}{dt} - -r_p[IL6 - IL6R - JAK]c$	r_p=0.3			
	B-6	$\frac{d[IL6 \quad IL6R \quad JAKP \quad STAT3]c}{dt} = k_1[IL6 - IL6R - JAKP]c[STAT3]c - k_{-1}[IL6 - IL6R - JAKP - STAT3]c$ $\frac{d[IL6 - IL6R - JAKP]c}{dt} = -k_1[IL6 - IL6R - JAKP]c[STAT3]c + k_{-1}[IL6 - IL6R - JAKP - STAT3]c$ $\frac{d[STAT3]c}{dt} - -k_1[IL6 - IL6R - JAKP]c[STAT3]c + k_{-1}[IL6 - IL6R - JAKP - STAT3]c$	k_1=8x10^8	k_{-1}=0.8	K_d=100nM	
	B-7	$\frac{d[IL6 \quad IL6R \quad JAKP \quad STAT3P]c}{dt} - r_p[IL6 - IL6R - JAKP - STAT3]c$ $\frac{d[IL6 \quad IL6R \quad JAKP \quad STAT3]c}{dt} - -r_p[IL6 - IL6R - JAKP - STAT3]c$	r_p=2			
	B-8	$\frac{d[IL6 \quad IL6R \quad JAKP \quad STAT3P]c}{dt} = k_1[IL6 - IL6R - JAKP]c[STAT3P]c - k_{-1}[IL6 - IL6R - JAKP - STAT3P]c$ $\frac{d[IL6 \quad IL6R \quad JAKP]c}{dt} = -k_1[IL6 - IL6R - JAKP]c[STAT3P]c + k_{-1}[IL6 - IL6R - JAKP - STAT3P]c$ $\frac{d[STAT3P]c}{dt} - -k_1[IL6 - IL6R - JAKP]c[STAT3P]c + k_{-1}[IL6 - IL6R - JAKP - STAT3P]c$	k_1=5x10^8	k_{-1}=0.5	K_d=100nM	
	B-9	$\frac{d[STAT3P \quad STAT3P]c}{dt} - k_2([STAT3P]c)^2 - k_{-1}[STAT3P - STAT3P]c$ $\frac{d[STAT3P]c}{dt} - 2(-k_2([STAT3P]c)^2 + k_{-1}[STAT3P - STAT3P]c)$	k_1=2x10^7	k_{-1}=0.1	K_d=5nM	
	B-10	$\frac{d[STAT3P \quad STAT3P]n}{dt} = r_m[STAT3P - STAT3P]c$ $\frac{d[STAT3P \quad STAT3P]c}{dt} - -r_{1m}[STAT3P - STAT3P]c$	r_m=0.1			
	B-11	$\frac{d[IL6 \quad IL6R \quad JAKP \quad SHP]c}{dt} = k_1[IL6 - IL6R - JAKP]c[SHP]c - k_{-1}[IL6 - IL6R - JAKP - SHP]c$ $\frac{d[IL6 \quad IL6R \quad JAKP]c}{dt} - -k_1[IL6 - IL6R - JAKP]c[SHP]c + k_{-1}[IL6 - IL6R - JAKP - SHP]c$ $\frac{d[SHP]c}{dt} - -k_1[IL6 - IL6R - JAKP]c[SHP]c + k_{-1}[IL6 - IL6R - JAKP - SHP]c$	k_1=10^8	k_{-1}=0.2	K_d=200nM	
	B-12	$\frac{d[IL6 \quad IL6R \quad JAK \quad SHP]c}{dt} - r_d[IL6 - IL6R - JAKP - SHP]c$ $\frac{d[IL6 \quad IL6R \quad JAKP \quad SHP]c}{dt} - -r_d[IL6 - IL6R - JAKP - SHP]c$	r_d=0.2			
	B-13	$\frac{d[IL6 - IL6R - JAK - SHP]c}{dt} - k_1[IL6 - IL6R - JAK]c[SHP]c - k_{-1}[IL6 - IL6R - JAK - SHP]c$ $\frac{d[IL6 \quad IL6R \quad JAK]c}{dt} - -k_1[IL6 - IL6R - JAK]c[SHP]c + k_{-1}[IL6 - IL6R - JAK - SHP]c$ $\frac{d[SHP]c}{dt} - -k_1[IL6 - IL6R - JAK]c[SHP]c + k_{-1}[IL6 - IL6R - JAK - SHP]c$	k_1=10^5	k_{-1}=0.2,	K_d=2mM	

Table 1. (*Continued*)

	B-14	$\frac{d[PPX\_STAT3P]c}{dt} = k_1[PPX]c[STAT3P]c - k_{-1}[PPX-STAT3P]c$ $\frac{d[PPX]c}{dt} = -k_1[PPX]c[STAT3P]c + k_{-1}[PPX\_STAT3P]c$ $\frac{d[STAT3P]c}{dt} = -k_1[PPX]c[STAT3P]c + k_{-1}[PPX\_STAT3P]c$	$k_1=10^8$	$k_{-1}=0.2$	$K_d=200nM$
	B-15	$\frac{d[PPX\_STAT3]c}{dt} = r_d[PPX-STAT3P]c$ $\frac{d[PPX\_STAT3P]c}{dt} = -r_d[PPX-STAT3P]c$	$r_d=0.2$		
	B-16	$\frac{d[PPX\_STAT3]c}{dt} = k_1[PPX]c[STAT3]c - k_{-1}[PPX-STAT3]c$ $\frac{d[PPX]c}{dt} = -k_1[PPX]c[STAT3]c + k_{-1}[PPX-STAT3]c$ $\frac{d[STAT3]c}{dt} = -k_1[PPX]c[STAT3]c + k_{-1}[PPX-STAT3]c$	$k_1=10^4$	$k_{-1}=0.2$	$K_d=20nM$
	B-17	$\frac{d[STAT3P-STAT3P]n}{dt} = k_1([STAT3P]n)^2 - k_{-1}[STAT3P-STAT3P]n$ $\frac{d[STAT3P]n}{dt} = 2(-k_1([STAT3P]n)^2 + k_{-1}[STAT3P-STAT3P]n)$	$k_1=2x10^7$	$k_{-1}=0.1,$	$K_d=5nM$
	B-18	$\frac{d[PPN\_STAT3P]n}{dt} = k_1[PPN]n[STAT3P]n - k_{-1}[PPN-STAT3P]n$ $\frac{d[PPN]n}{dt} = -k_1[PPN]n[STAT3P]n + k_{-1}[PPN-STAT3P]n$ $\frac{d[STAT3P]n}{dt} = -k_1[PPN]n[STAT3P]n + k_{-1}[PPN-STAT3P]n$	$k_1=10^8$	$k_{-1}=0.2$	$K_d=200nM$
	B-19	$\frac{d[PPN\_STAT3]n}{dt} = r_d[PPN-STAT3P]n$ $\frac{d[PPN\_STAT3P]n}{dt} = -r_d[PPN-STAT3P]n$	$r_d=0.3$		
	B-20	$\frac{d[PPN\_STAT3]n}{dt} = k_1[PPN]n[STAT3]n - k_{-1}[PPN-STAT3]n$ $\frac{d[PPN]n}{dt} = -k_1[PPN]n[STAT3]n + k_{-1}[PPN-STAT3]n$ $\frac{d[STAT3]n}{dt} = -k_1[PPN]n[STAT3]n + k_{-1}[PPN\_STAT3]n$	$k_1=10^4$	$k_{-1}=0.2$	$K_d=20nM$
	B-21	$\frac{d[STAT3]c}{dt} = r_m[STAT3]n$ $\frac{d[STAT3]n}{dt} = -r_{1m}[STAT3]n$	$r_m=0.3$		
	B-22	$\frac{d[SOCS]c}{dt} = r_s[NFkBP\_STAT3P\_STAT3P]n$	$r_s=0.002$		
	B-23	$\frac{d[SOCS]c}{dt} = r_s[STAT3P-STAT3P]n$	$r_s=0.0004$		
	B-24	$\frac{d[IL6\_IL6R\_JAKP\_SOCS]c}{dt} = k_1[IL6-IL6R-JAKP]c[SOCS]c - k_{-1}[IL6-IL6R-JAKP-SOCS]c$ $\frac{d[IL6\_IL6R\_JAKP]c}{dt} = -k_1[IL6-IL6R-JAKP]c[SOCS]c + k_{-1}[IL6-IL6R-JAKP-SOCS]c$ $\frac{d[SOCS]c}{dt} = -k_1[IL6\_IL6R\_JAKP\_SOCS]c + k_{-1}[IL6\_IL6R\_JAKP\_SOCS]c$	$k_1=10^8$	$k_{-1}=1$	$K_d=10nM$
IL-6 production	BA-1	$\frac{d[mRNAIL6]n}{dt} = k_f \frac{[NFkBP-STAT3P-STAT3P]n}{K_t + [NFkBP\_STAT3P\_STAT3P]n}$	$k_f=2x10^{-12}$	$Kt=200nM$	
	BA-2	$\frac{d[mRNAIL6]c}{dt} = r_m[mRNAIL6]n$ $\frac{d[mRNAIL6]n}{dt} = -r_m[mRNAIL6]n$	$r_m=0.02$		
	BA-3	$\frac{d[IL6]e}{dt} = r_s[mRNAIL6]c$	$r_s=0.02$		
	BA-4	$\frac{d[IL6]j}{dt} = (r_m[IL6]e)\frac{1}{r}$ $\frac{d[IL6]e}{dt} = -r_m[IL6]e$	$r_m=0.03$	$r=30$	
IL-6 receptor production	BB-1	$\frac{d[mRNAIL6R]n}{dt} = k_f \frac{[NFkBP\_STAT3P\_STAT3P]n}{K_t + [NFkBP-STAT3P-STAT3P]n}$	$k_f=2x10^{-12}$	$Kt=200nM$	
	BB-2	$\frac{d[mRNAIL6R]c}{dt} = r_m[mRNAIL6R]n$ $\frac{d[mRNAIL6R]n}{dt} = -r_m[mRNAIL6R]n$	$r_m=0.02$		

Table 1. (*Continued*)

	BB-3	$\frac{d[IL6R]e}{dt} - r_s[mRNAIL6R]c$	r_s=0.02
	BB-4	$\frac{d[IL6R]c}{dt} = r_m[IL6R]e$ $\frac{d[IL6R]e}{dt} = -r_m[IL6R]e$	r_m=0.002
IL-6 receptor internalization	BC-1	$\frac{d[IL6R]i}{dt} - r_i\left(e_1 + (1-e_1)\left(1-e^{\frac{-3t}{T_1}}\right)\right)[IL6R]c$ $\frac{d[IL6R]c}{dt} - -r_i\left(e_1 + (1-e_1)\left(1-e^{\frac{-3t}{T_1}}\right)\right)[IL6R]c$	r_i=0.00016 e_1=0.12 T_1=35
	BC-2	$\frac{d[IL6R\quad JAK]i}{dt} - r_i\left(e_1 + (1-e_1)\left(1-e^{\frac{-3t}{T_1}}\right)\right)[IL6R-JAK]c$ $\frac{d[IL6R\quad JAK]c}{dt} - -r_i\left(e_1 + (1-e_1)\left(1-e^{\frac{-3t}{T_1}}\right)\right)[IL6R-JAK]c$	r_i=0.0024 e_1=0.12 T_1=35
	BC-3	$\frac{d[IL6\quad IL6R\quad JAK]i}{dt} - r_i\left(e_1 + (1-e_1)\left(1-e^{\frac{-3t}{T_1}}\right)\right)[IL6-IL6R-JAK]c$ $\frac{d[IL6\quad IL6R\quad JAK]c}{dt} - -r_i\left(e_1 + (1-e_1)\left(1-e^{\frac{-3t}{T_1}}\right)\right)[IL6-IL6R-JAK]c$	r_i=0.012 e_1=0.12 T_1=35
	BC-4	$\frac{d[IL6\quad IL6R\quad JAKP]i}{dt} - r_i\left(e_1 + (1-e_1)\left(1-e^{\frac{-3t}{T_1}}\right)\right)[IL6-IL6R-JAKP]c$ $\frac{d[IL6-IL6R-JAKP]c}{dt} - -r_i\left(e_1 + (1-e_1)\left(1-e^{\frac{-3t}{T_1}}\right)\right)[IL6-IL6R-JAKP]c$	r_i=0.004 e_1=0.12 T_1=35
	BC-5	$\frac{d[IL6R]c}{dt} = r_m[IL6R]i$ $\frac{d[IL6R]i}{dt} = -r_m[IL6R]i$	r_m=0.0012
NFkB–STAT3 complex formation	C-1	$\frac{d[NFkBP\quad STAT3P\quad STAT3P]c}{dt} = k_1[NFkBP]c[STAT3P-STAT3P]c - k_{-1}[NFkBP-STAT3P-STAT3P]c$ $\frac{d[NFkBP]c}{dt} - k_1[NFkBP]c[STAT3P\quad STAT3P]c + k_{-1}[NFkBP\quad STAT3P\quad STAT3P]c$ $\frac{d[STAT3P\quad STAT3P]c}{dt} - -k_1[NFkBP]c[STAT3P-STAT3P]c + k_{-1}[NFkBP-STAT3P-STAT3P]c$	k_1=2x 10^9 k_{-1}=100 K_d=50nM
	C-1b	$\frac{d[NFkBP\quad STAT3P\quad STAT3P]n}{dt} = k_1[NFkBP]n[STAT3P-STAT3P]n - k_{-1}[NFkBP-STAT3P-STAT3P]n$ $\frac{d[NFkBP]n}{dt} - -k_1[NFkBP]n[STAT3P-STAT3P]n + k_{-1}[NFkBP-STAT3P-STAT3P]n$ $\frac{d[STAT3P-STAT3P]n}{dt} - -k_1[NFkBP]n[STAT3P-STAT3P]n + k_{-1}[NFkBP-STAT3P-STAT3P]n$	k_1=2x 10^9 k_{-1}=100 K_d=50nM
	C-2	$\frac{d[NFkBP\quad STAT3P\quad STAT3P]n}{dt} = r_m[NFkBP-STAT3P-STAT3P]c$ $\frac{d[NFkBP\quad STAT3P\quad STAT3P]c}{dt} = -r_m[NFkBP-STAT3P-STAT3P]c$	r_m=0.00005
	C-3	$\frac{d[NFkBP\quad STAT3P\quad STAT3P]c}{dt} = r_m[NFkBP-STAT3P-STAT3P]n$ $\frac{d[NFkBP\quad STAT3P\quad STAT3P]n}{dt} - \quad r_m[NFkBP\quad STAT3P\quad STAT3P]n$	r_m=0.00005
Cytokine production	D-1	$\frac{d[epiregulin]j}{dt} - (r_s[synovial]j)\frac{[NFkBP-STAT3P-STAT3P]n}{K_t + [NFkBP\quad STAT3P\quad STAT3P]n}$	r_s=800 K_t=5nM
	D-2	$\frac{d[CCL2]j}{dt} - (r_s[synovial]j)\frac{[NFkBP-STAT3P-STAT3P]n}{K_t + [NFkBP\quad STAT3P\quad STAT3P]n}$	r_s=100 K_t=5nM
	D-3	$\frac{d[CCL20]j}{dt} - (r_s[synovial]j)\frac{[NFkBP\quad STAT3P\quad STAT3P]n}{K_t + [NFkBP-STAT3P-STAT3P]n}$	r_s=20 K_t=5nM
	D-4	$\frac{d[IL\quad 17]j}{dt} = r_s[Th17]j$	r_s=100
	D-5	$\frac{d[IL6]j}{dt} - r_s[macrophage]j$	r_s=400
	D-6	$\frac{d[TNF]j}{dt} - r_s[macrophage]j$	r_s=10
	D-7	$\frac{d[CCL20]j}{dt} = r_s[macrophage]j$	r_s=20
Cell movement	E-1	$\frac{d[Th17]j}{dt} - (r_m[Th17]b)\frac{[CCL20]j}{K_m + [CCL20]j}$	r_m=0.00012 K_m=10nM
	E-2	$\frac{d[macrophage]j}{dt} - (r_m[macrophage]b)\frac{[CCL2]j}{K_m + [CCL2]j}$	r_m=0.00012 K_m=10nM
Proliferation	F-1	$\frac{d[synovial]j}{dt} - (r_i[synovial]j)(r + (1-r)\frac{[epiregulin]j}{K_{m1} + [epiregulin]j})\frac{[NFkBP-STAT3P-STAT3P]n}{K_{m2} + [NFkBP-STAT3P-STAT3P]n}$	r_i=0.0002 K_{m1}=1nM r=0.6 K_{m2}=5nM

539 **Table 1. (*Continued*)**

Cell death	G-1	$\frac{d[synovial]_j}{dt} - (-r_e[synovial]_j)(r + (1-r)\frac{[synovial]_j}{K_m + [synovial]_j})$	r_e=0.0006 K_m=20fM r=0.07
	G-2	$\frac{d[Th17]_j}{dt} - (-r_e[Th17]_j)(r + (1-r)\frac{[Th17]_j}{K_m + [Th17]_j})$	r_e=0.0004 K_m=20fM r=0.1
	G-3	$\frac{d[macrophage]_j}{dt} - (-r_e[macrophage]_j)(r + (1-r)\frac{[macrophage]_j}{K_m + [macrophage]_j})$	r_e=0.0002 K_m=20fM r=0.1
Degradation	H-1	$\frac{d[IkBaP]_c}{dt} = -r_e[IkBaP]_c$	r_e=0.005
	H-2	$\frac{d[IKKP]_c}{dt} = -r_e[IKKP]_c$	r_e=0.005
	H-3	$\frac{d[IL\_17]_j}{dt} = -r_e[IL-17]_j$	r_e=0.00002
	H-4	$\frac{d[TNF]_j}{dt} - r_e[TNF]_j$	r_e=0.0005
	H-5	$\frac{d[IL6]_j}{dt} - r_e[IL6]_j$	r_e=0.00004
	H-6	$\frac{d[epiregulin]_j}{dt} = -r_e[epiregulin]_j$	r_e=0.0005
	H-7	$\frac{d[mRNAIL6]_c}{dt} = -r_e[mRNAIL6]_c$	r_e=0.001
	H-8	$\frac{d[mRNAIL6R]_c}{dt} = -r_e[mRNAIL6R]_c$	r_e=0.0005
	H-9	$\frac{d[IL6R]_i}{dt} - r_e[IL6R]_i$	r_e=0.00005
	H-10	$\frac{d[SOCS]_c}{dt} = -r_e[SOCS]_c$	r_e=0.0005
	H-11	$\frac{d[CCL2]_j}{dt} = -r_e[CCL2]_j$	r_e=0.0002
	H-12	$\frac{d[CCL20]_j}{dt} = -r_e[CCL20]_j$	r_e=0.0005
Initial concentration		[synovial]j	1.204×10^8 cells/ml = 2 fM
		[Th17]b	1.204×10^8 cells/ml = 2 fM
		[macrophage]b	1.204×10^8 cells/ml = 2 fM
		[NFkB]c	0.2 nM
		[IkBa]c	100 nM
		[NFkB-IkBa]c	200 nM
		[IL6]j	1pM
		[IL6R]c	4 nM
		[JAK]c	8 nM
		[STAT3]c	800 nM
		[SHP]c	100 nM
		[PPX]c	50 nM
		[PPN]n	60 nM
		[CCL20]j	2 nM
		[CCL2]j	0.5 nM

The [x]b, [x]j, [x]c, [x]n , [x]e, and [x]i indicate the concentration of factor x in blood, joint, cytoplasm of synovial cells, nucleus of synovials cell, ER of synovial cells, and internalized receptors, respectively.

k_t, K_m, k_1, k_{-1}, K_d, r_p, r_d, r_m, K_q, r_s, r_i, r_l, and r_e denote the rate constant for production, the dissociation constant for cytokine, the rate constnt for binding, the rate constant for dissociation, the dissociation constant, the rate constant for phosphorylation, the rate constant for dephosphorylation, the rate constant for movement, the dissociation constant for transcription, the rate constant for synthesis, the rate constant for internalization, the rate constant for proliferation, and the rate constant for degradation, respectively.

In F759 cells, reaction "B-24" is excluded.

In this system, the base time unit is minute.

The initial concentrations of all other factors are 0.

540
541

Acknowledgments

We appreciate the excellent technical assistance provided by Ms. Taru, Dr. Ishii, and Ms. Nakayama and thank Ms. Yamamoto, Ms. Morita, and Ms. Ohsawa for their excellent assistance. We thank Sofia Science Writing for carefully reading the manuscript. This work was supported by KAKENHI (#21H05044 and #22K1944 to A.Y.; #20H00502 and #21K19364 to M.M.), Quantum LEAP Flagship Program (#JPMXS0120330644 to M.M.), Agency for Medical Research and Development (AMED) (#JP22ek0510030 and #JP223fa627005 to M.M.), AMED-CREST (#JP20gm1110009 to A.Y.), and AMED Moonshot (#21zf0127003h0001 to A.Y., #JP21zf0127004 to M.M.). This work was also supported by the Grant for Joint Research Program of the Institute for Genetic Medicine from Hokkaido University, Photo-excitonix Project from Hokkaido University, and the Promotion Project for Young Investigators from Hokkaido University (M.M.).

Author Contributions

D.K., A.Y., and M.M. designed the study. R.Y., S.Y., and T.A. performed the majority of experiments. Shigeru.H., K.M., A.H., S.N., Shintaro.H., Y.T., I.O., J.-J. J. Y.S., and S.K. contributed to specific experiments. N.I., and Shigeru.H. advised on the research design. S.Y., Shigeru.H., and M.M. wrote and edited the manuscript. S.Y., Shigeru.H., and M.M. supervised the study.

Declaration of competing interest

The authors declare they have no conflicting financial interests.

Data availability

Data will be made available upon reasonable request.

References

[1] G.S. Firestein, Evolving concepts of rheumatoid arthritis, Nature 423 (6937) (2003) 356-361, doi: 10.1038/nature01661.

[2] M. Murakami, D. Kamimura, T. Hirano, Pleiotropy and Specificity: Insights from the Interleukin 6 Family of Cytokines, Immunity 50 (4) (2019) 812-831, doi: 10.1016/j.immuni.2019.03.027.

[3] T. Atsumi, K. Ishihara, D. Kamimura, et al., A point mutation of Tyr-759 in interleukin 6 family cytokine receptor subunit gp130 causes autoimmune arthritis, J. Exp. Med. 196 (7) (2002) 979-990, doi: 10.1084/jem.20020619.

[4] S. Sawa, D. Kamimura, G. Jin, et al., Autoimmune arthritis associated with mutated IL-6 receptor gp130 is driven by STAT3/IL-7-dependent homeostatic proliferation of CD4+ T cells, J. Exp. Med. 203 (6) (2006) 1459-1470, doi: 10.1084/jem.20052187.

[5] M. Murakami, Y. Okuyama, H. Ogura, et al., Local microbleeding facilitates IL-6–and IL-17–dependent arthritis in the absence of tissue antigen recognition by activated T cells, J. Exp. Med. 208 (1) (2011) 103-114, doi: 10.1084/jem.20100900.

[6] H. Ogura, M. Murakami, Y. Okuyama, et al., Interleukin-17 Promotes Autoimmunity by Triggering a Positive-Feedback Loop via Interleukin-6 Induction, Immunity 29 (4) (2008) 628-636, doi: 10.1016/j.immuni.2008.07.018.

[7] M. Harada, D. Kamimura, Y. Arima, et al., Temporal Expression of Growth Factors Triggered by Epiregulin Regulates Inflammation Development, J. Immunol. 194 (3) (2015) 1039-1046, doi: 10.4049/jimmunol.1400562.

[8] J. Meng, J.-J. Jiang, T. Atsumi, et al., Breakpoint cluster region-mediated inflammation is dependent on casein kinase II, J. Immunol. 197 (8) (2016) 3111-3119, doi: 10.4049/jimmunol.1601082.

[9] M. Murakami, M. Harada, D. Kaminura, et al., Disease-association analysis of an inflammation-related feedback loop, Cell Rep. 3 (3) (2013) 946-959, doi: 10.1016/j.celrep.2013.01.028.

[10] R. Hasebe, K. Murakami, M. Harada, et al., ATP spreads inflammation to other limbs through crosstalk between sensory neurons and interneurons, J Exp Med. 219 (6) (2022) e20212019, doi: 10.1084/jem.20212019.

[11] A. Stofkova, D. Kamimura, T. Ohki, et al., Photopic light-mediated down-regulation of local α1A-adrenergic signaling protects blood-retina barrier in experimental autoimmune uveoretinitis, Sci Rep. 9 (1) (2019) 2353, doi: 10.1038/s41598-019-38895-y.

[12] Y. Arima, M. Harada, D. Kamimura, et al., Regional neural activation defines a gateway for autoreactive T cells to cross the blood-brain barrier, Cell 148 (3) (2012) 447-457, doi: 10.1016/j.cell.2012.01.022.

[13] Y. Arima, T. Ohki, N. Nishikawa, et al., Brain micro-inflammation at specific vessels dysregulates organ-homeostasis via the activation of a new neural circuit, Elife 6 (2017) e25517, doi: 10.7554/eLife.25517.

[14] T. Atsumi, H. Suzuki, J.-J. Jiang, et al., Rbm10 regulates inflammation development via alternative splicing of Dnmt3b, Int Immunol. 29 (12) (2017) 581-591, doi: 10.1093/intimm/dxx067.

[15] Y. Tanaka, L. Sabharwal, M. Ota, et al., Presenilin 1 Regulates NF-κB Activation via Association with Breakpoint Cluster Region and Casein Kinase II, J Immunol. 201 (8) (2018) 2256-2263, doi: 10.4049/jimmunol.1701446.

[16] Y. Okuyama, Y. Tanaka, J.-J. Jiang, et al., Bmi1 Regulates IκBα Degradation via Association with the SCF Complex, J Immunol. 201 (8) (2018) 2264-2272, doi: 10.4049/jimmunol.1701223.
[17] M. Fujita, Y. Yamamoto, J.-J. Jiang, et al., NEDD4 Is Involved in Inflammation Development during Keloid Formation, J Invest Dermatol. 139 (2) (2019) 333-341, doi: 10.1016/j.jid.2018.07.044.
[18] H. Tanaka, Y. Arima, D. Kamimura, et al., Phosphorylation-dependent Regnase-1 release from endoplasmic reticulum is critical in IL-17 response, J Exp Med. 216 (6) (2019) 1431-1449, doi: 10.1084/jem.20181078.
[19] M. Ota, Y. Tanaka, I. Nakagawa, et al., Role of Chondrocytes in the Development of Rheumatoid Arthritis Via Transmembrane Protein 147-Mediated NF-κB Activation, Arthritis Rheumatol. 72 (6) (2020) 931-942. doi: 10.1002/art.41182.
[20] H. Higuchi, D. Kamimura, J.-J. Jiang, et al., Orosomucoid 1 is involved in the development of chronic allograft rejection after kidney transplantation, Int Immunol. 32 (5) (2020) 335-346, doi: 10.1093/intimm/dxaa003.
[21] S. Shimoyama, I. Nakagawa, J.-J. Jiang, et al., Sjögren's syndrome-associated SNPs increase GTF2I expression in salivary gland cells to enhance inflammation development, Int Immunol. 33 (8) (2021) 423-434, doi: 10.1093/intimm/dxab025.
[22] Y. Takada, D. Kamimura, J.-J. Jiang, et al., Increased urinary exosomal SYT17 levels in chronic active antibody-mediated rejection after kidney transplantation via the IL-6 amplifier, Int Immunol. 32 (10) (2020) 653-662, doi: 10.1093/intimm/dxaa032.
[23] J. Lee, T. Nakagiri, T. Oto, et al., IL-6 amplifier, NF-κB-triggered positive feedback for IL-6 signaling, in grafts is involved in allogeneic rejection responses, J Immunol. 189 (4) (2012) 1928-1936, doi: 10.4049/jimmunol.1103613.
[24] J. Lee, T. Nakagiri, D. Kamimura, et al., IL-6 amplifier activation in epithelial regions of bronchi after allogeneic lung transplantation, Int Immunol. 25 (5) (2013) 319-332, doi: 10.1093/intimm/dxs158.
[25] Y. Arima, D. Kamimura, T. Atsumi, et al., A pain-mediated neural signal induces relapse in murine autoimmune encephalomyelitis, a multiple sclerosis model, Elife 4 (2015) e08733, doi: 10.7554/eLife.08733.
[26] H.J. Wang, C.P. Su, C.C. Lai, et al., Deep Learning-Based Computer-Aided Diagnosis of Rheumatoid Arthritis with Hand X-ray Images Conforming to Modified Total Sharp/van der Heijde Score, Biomedicines. 10(6) (2022)1355, doi: 10.3390/biomedicines10061355.
[27] B. Norgeot, B.S. Glicksberg, L. Trupin, et al., Assessment of a Deep Learning Model Based on Electronic Health Record Data to Forecast Clinical Outcomes in Patients With Rheumatoid Arthritis, JAMA Netw Open, 2(3) (2019) e190606, doi: 10.1001/jamanetworkopen.2019.0606.
[28] C. J. Proctor, C. Macdonald, J.M. Milner, et al., A computer simulation approach to assessing therapeutic intervention points for the prevention of cytokine-induced cartilage breakdown, Arthritis Rheumatol. 66(4) (2014) 979-989, doi: 10.1002/art.38297.
[29] S. Yamada, S. Shiono, A. Joo, A. Yoshimura, A. Control mechanism of JAK/STAT signal transduction pathway, FEBS Lett. 534 (1-3) (2003) 190-196, doi: 10.1016/s0014-5793(02)03842-5.

[30] S. Yamada, J. Tsukada, A. Yoshimura, M. Kubo, Computer simulation of the role of SOCS family protein in helper T cell differentiation, Int. Immun. 18 (2) (2006) 335-345, doi: 10.1093/intimm/dxh372.
[31] S. Yamada, T. Taketomi, A. Yoshimura, Model analysis of difference between EGF pathway and FGF pathway, Biochim. Biophys. Res. Commun. 314 (4) (2004) 1113-1120, doi: 10.1016/j.bbrc.2004.01.009.
[32] A. Kerschbaumer, A. Sepriano, J.S. Smolen, et al., Efficacy of pharmacological treatment in rheumatoid arthritis: a systematic literature research informing the 2019 update of the EULAR recommendations for management of rheumatoid arthritis, Ann Rheum Dis. 79 (6) (2020) 744-759, doi: 10.1136/annrheumdis-2019-216656.
[33] A. Saltelli, K. Chan, E.M. Scott, eds. 2000, Sensitivity Analysis, John Willey & Sons Inc.
[34] Ogura H, Atsumi T, Bando H, et al., The reverse-direction method links mass experimental data to human diseases, Arch Immunol Ther Exp (Warsz). 62(1) (2014) 41-45, doi: 10.1007/s00005-013-0255-9.
[35] McInnes IB, Schett G, Pathogenetic insights from the treatment of rheumatoid arthritis, Lancet. 389(10086) (2017) 2328-2337. doi: 10.1016/S0140-6736(17)31472-1.
[36] J.S. Smolen, S. D. Aletaha, Rheumatoid arthritis therapy reappraisal: strategies, opportunities and challenges, Nat Rev Rheumatol. 11 (5) (2015) 276-289, doi: 10.1038/nrrheum.2015.8.
[37] T. Yi, H.L. Lee, J.H. Cha, et al., Epidermal growth factor receptor regulates osteoclast differentiation and survival through cross-talking with RANK signaling, J. Cell Physiol. 217 (2) (2008) 409-422, doi: 10.1002/jcp.21511.
[38] M. Feldmann, R.N. Maini, Anti-TNF alpha therapy of rheumatoid arthritis: what have we learned? Annu Rev Immunol. 19 (2001) 163-196, doi: 10.1146/annurev.immunol.19.1.163.

Figure Legends

Fig. 1. Association of STAT3 and NF-kB in nonimmune cells.
A. HEK293T cells bearing HA-p65, mock, or STAT3-Flag were separated into cytosolic and nuclear fractions. Immunoprecipitation was performed to measure the p65-STAT3 complex in the cytoplasmic and nuclear fractions. Anti-a-Tubulin and anti-Lamin-A/C antibodies were used as cytosolic and nuclear markers, respectively. **B-D.** ATAC-seq Peak Browser images depicting the promoter regions of IL-6 (B), CCL2 (C), and epiregulin (D) with or without IL-6 amplifier (Amp) activation in wild-type (B6) and F759 fibroblasts. Using ChIP-Atlas, the NF-kB (RelA), STAT3, and RNA polymerase II (Pol II) binding regions were visualized on these genomic loci.

Fig. 2. Signaling pathways and reactions in the simulation model of F759 arthritis.
A. Intracellular reactions in synovial fibroblasts. **B.** Molecular interactions among cells from blood in the joints. For a detailed explanation of the reactions, see Materials and Methods and Table 1.

Fig. 3. Concentration dependency of IL-6 mRNA in steady state.
A. *In silico* results. **B.** *In vitro* results. Open bars: wild-type, closed bars: F759 mice. The concentrations of IL-6 in the top right graph is 0-10 pM (A) and 0-6 relative to IL-6 mRNA expression (B). Data in B are representative of at least 3 independent experiments and indicate the mean + SEM. ★, $P<0.05$. Student's t tests (two-tailed).

Fig. 4. Time course of different factors during IL-6 amplifier activation.
A. *In silico* time course of the STAT3-NF-kB complex formation. **B.** *In vitro* time course of STAT3 binding to the IL-6 promotor in cultured synovial fibroblasts. **C.** *In silico* time course of IL-6 mRNA in the cytoplasm. **D.** *In vitro* time course of IL-6 mRNA in cultured synovial fibroblasts. Open triangles: wild-type, closed circles: F759 mice. Data in B and D are representative of at least 3 independent experiments and indicate the mean + SEM. ★, $P<0.05$. Student's t tests (two-tailed).

Fig. 5. *In silico* dependency of IL-6 expression on IL-6 and IL-17 concentrations in the joints of F759 mice in steady state. The dependency in the presence (A) and absence (B) of the STAT3-NF-kB complex. The concentration of IL-6 was 0-0.25 nM (top right graphs).

Fig. 6. *In silico* dependency of IL-6 expression on Th17 cell and macrophage concentrations in the blood of F759 mice in the presence (A) and absence (B) of the STAT3-NF-kB complex in steady state.
The concentration of IL-6 was 0-0.25 nM (top right graphs).

Fig. 7. *In silico* expression of different factors.
A. Wild-type mice. **B.** F759 mice. Log-scale plot was used for Y-axis.

Fig. 8. *In silico* effects of anti-cytokine antibodies.
A. No antibody treatment. **B.** Anti-IL-6 antibody treatment at day 250. **C.** Anti-TNFα antibody treatment at day 250. **D.** Anti-IL-17 antibody treatment at day 250. **E.** Anti-TNFα and anti-IL-17 antibody combination treatment at day 250. **F.** Epiregulin levels at

day 300 following treatment at day 50. **G.** Anti-IL-17 antibody treatment at day 50. **H.** Anti-IL-17 antibody treatment at day 100. Red arrowheads indicate antibody dosing time. Log-scale plot was used for Y-axis (A-E, G-H).

Fig. 9. *Sensitivity analysis in silico.*
A. The x-axis shows normalized log scales from 0.1 to 10 for different parameters, and the y-axis shows the relative epiregulin production. The dotted lines are tangents to the epiregulin production. "Sensitivity" is defined as the slope of the tangents.
a. The dissociation constant (K_d) between IL-17 and its receptor. **b.** K_d between NF-kB and IkBα. **c.** The rate constant for the phosphorylation (r_p) of IkBα. **d.** r_p of NF-kB. **e.** K_d between activated NF-kB and activated STAT3. **f.** The rate constant for the movement (r_m) of the STAT3-NF-kB complex from the cytoplasm to the nucleus. **g.** r_m of NF-kB/STAT3 from the nucleus to the cytoplasm. **h.** K_d between NF-kB and IkBα transcription (K_t). **i.** r_m of IkBα from the nucleus to the cytoplasm. **j.** K_t between the STAT3-NF-kB complex and IL-6 transcription. **k.** K_t between the STAT3-NF-kB complex and epiregulin transcription. **l.** K_t between the STAT3-NF-kB complex and CCL20 transcription. **m.** K_t between the STAT3-NF-kB complex and the CCL2 transcription site. **n.** K_t between the STAT3-NF-kB complex and the synovial cell proliferation site. **o.** K_d between IL-6 and its receptor. **p.** r_p of STAT3. **q.** The rate constant of the synthesis (r_s) of IL-17 by Th17 cells. **r.** r_s of IL-6 by macrophages. **s.** r_s of TNFα by macrophages. **t.** r_m of Th17 cells from the blood to the joint. **u.** The dissociation constant on the effect of the movement (K_m) of Th17 cells from the blood to the joints in response to CCL20. **v.** r_m of macrophages from the blood to the joint in response to CCL20. **w.** K_m of macrophages from the blood to the joint in response to CCL2. **x.** r_s of CCL20 by macrophages.

B. The sensitivity of each parameter.

Fig. S1. *In silico* effects of anti-cytokine antibodies.
A. Anti-IL-6 antibody treatment at day 50. **B.** Anti-TNFα antibody treatment at day 50. Red arrowheads indicate antibody dosing time.

Table 1 Differential equations for biochemical reactions and kinetic parameters

Pathway	No.	differential equations	parameters
NFkB activating pathway	A-1	$\frac{d[IKKP]c}{dt} = k_f \frac{[IL-17]j}{K_m + [IL-17]j}$	k_f=5x10^{-10} K_m=5nM
	A-2	$\frac{d[IKKP]c}{dt} = k_f \frac{[TNF]j}{K_m + [TNF]j}$	k_f=5x10^{-10} K_m=5nM
	A-3	$\frac{d[IKKP]c}{dt} = k_f \frac{[epiregulin]j}{K_m + [epiregulin]j}$	k_f=5x10^{-10} K_m=5nM
	A-4	$\frac{d[NFkB-IkBa]c}{dt} = k_1[NFkB]c[IkBa]c - k_{-1}[NFkB-IkBa]c$ $\frac{d[NFkB]c}{dt} = -k_1[NFkB]c[IkBa]c + k_{-1}[NFkB-IkBa]c$ $\frac{d[IkBa]c}{dt} = -k_1[NFkB]c[IkBa]c + k_{-1}[NFkB-IkBa]c$	k_1=5x10^8 k_{-1}=0.025 K_d=0.05nM
	A-5	$\frac{d[NFkBP-IkBa]c}{dt} = k_1[NFkBP]c[IkBa]c - k_{-1}[NFkBP-IkBa]c$ $\frac{d[NFkBP]c}{dt} = -k_1[NFkBP]c[IkBa]c + k_{-1}[NFkBP-IkBa]c$ $\frac{d[IkBa]c}{dt} = -k_1[NFkBP]c[IkBa]c + k_{-1}[NFkBP-IkBa]c$	k_1=5x10^7 k_{-1}=0.05 K_d=1nM

	A-6	$$\frac{d[IkBa-IKKP]c}{dt} = k_1[IkBa]c[IKKP]c - k_{-1}[IkBa-IKKP]c$$ $$\frac{d[IkBa]c}{dt} = -k_1[IkBa]c[IKKP]c + k_{-1}[IkBa-IKKP]c$$ $$\frac{d[IKKP]c}{dt} = -k_1[IkBa]c[IKKP]c + k_{-1}[IkBa-IKKP]c$$	$k_1=5x10^7$ $k_{-1}=0.05$ $K_d=1nM$
	A-7	$$\frac{d[IkBaP-IKKP]c}{dt} = r_p[IkBa-IKKP]c$$ $$\frac{d[IkBa-IKKP]c}{dt} = -r_p[IkBa-IKKP]c$$	$r_p=0.05$
	A-8	$$\frac{d[IkBaP-IKKP]c}{dt} = k_1[IkBaP]c[IKKP]c - k_{-1}[IkBaP-IKKP]c$$ $$\frac{d[IkBaP]c}{dt} = -k_1[IkBaP]c[IKKP]c + k_{-1}[IkBaP-IKKP]c$$ $$\frac{d[IKKP]c}{dt} = -k_1[IkBaP]c[IKKP]c + k_{-1}[IkBaP-IKKP]c$$	$k_1=10^7$ $k_{-1}=0.2$ $K_d=20nM$

	A-9	$$\frac{d[NFkB-IKKP]c}{dt} = k_1[NFkB]c[IKKP]c - k_{-1}[NFkB-IKKP]c$$ $$\frac{d[NFkB]c}{dt} = -k_1[NFkB]c[IKKP]c + k_{-1}[NFkB-IKKP]c$$ $$\frac{d[IKKP]c}{dt} = -k_1[NFkB]c[IKKP]c + k_{-1}[NFkB-IKKP]c$$	$k_1=5x10^7$ $k_{-1}=0.05$ $K_d=1nM$
	A-10	$$\frac{d[NFkBP-IKKP]c}{dt} = r_p[NFkB-IKKP]c$$ $$\frac{d[NFkB-IKKP]c}{dt} = -r_p[NFkB-IKKP]c$$	$r_p=0.005$
	A-11	$$\frac{d[NFkBP-IKKP]c}{dt} = k_1[NFkBP]c[IKKP]c - k_{-1}[NFkBP-IKKP]c$$ $$\frac{d[NFkBP]c}{dt} = -k_1[NFkBP]c[IKKP]c + k_{-1}[NFkBP-IKKP]c$$ $$\frac{d[IKKP]c}{dt} = -k_1[NFkBP]c[IKKP]c + k_{-1}[NFkBP-IKKP]c$$	$k_1=10^7$ $k_{-1}=0.2$ $K_d=20nM$
	A-12	$$\frac{d[NFkB]c}{dt} = r_d[NFkBP]c$$ $$\frac{d[NFkBP]c}{dt} = -r_d[NFkBP]c$$	$r_d=0.002$

	A-13	$\frac{d[NFkBP]n}{dt} = r_m[NFkBP]c$ $\frac{d[NFkBP]c}{dt} = -r_m[NFkBP]c$	r_m=0.002
	A-14	$\frac{d[NFkBP]c}{dt} = r_m[NFkBP]n$ $\frac{d[NFkBP]n}{dt} = -r_m[NFkBP]n$	r_m=0.001
	A-15	$\frac{d[IkBa]n}{dt} = k_f \frac{[NFkBP]n}{K_t + [NFkBP]n}$	k_f=2x10^{-9} K_t=2nM
	A-16	$\frac{d[IkBa]c}{dt} = r_m[IkBa]n$ $\frac{d[IkBa]n}{dt} = -r_m[IkBa]n$	r_m=0.01
STAT3 activating pathway	B-1	$\frac{d[IL6-IL6R]c}{dt} = k_1[IL6]j[IL6R]c - k_{-1}[IL6-IL6R]c$ $\frac{d[IL6]j}{dt} = (-k_1[IL6]j[IL6R]c + k_{-1}[IL6-IL6R]c)\frac{1}{r}$ $\frac{d[IL6R]c}{dt} = -k_1[IL6]j[IL6R]c + k_{-1}[IL6-IL6R]c$	k_1=2x10^6 k_{-1}=0.02 K_d=10nM r=30

	B-2	$$\frac{d[IL6R-JAK]c}{dt}=k_1[IL6R]c[JAK]c-k_{-1}[IL6R-JAK]c$$ $$\frac{d[IL6R]c}{dt}=-k_1[IL6R]c[JAK]c+k_{-1}[IL6R-JAK]c$$ $$\frac{d[JAK]c}{dt}=-k_1[IL6R]c[JAK]c+k_{-1}[IL6R-JAK]c$$	$k_1=10^8$ $k_{-1}=0.05$ $K_d=0.5nM$
	B-3	$$\frac{d[IL6-IL6R-JAK]c}{dt}=k_1[IL6-IL6R]c[JAK]c-k_{-1}[IL6-IL6R-JAK]c$$ $$\frac{d[IL6-IL6R]c}{dt}=-k_1[IL6-IL6R]c[JAK]c+k_{-1}[IL6-IL6R-JAK]c$$ $$\frac{d[JAK]c}{dt}=-k_1[IL6-IL6R]c[JAK]c+k_{-1}[IL6-IL6R-JAK]c$$	$k_1=10^8$ $k_{-1}=0.05$ $K_d=0.5nM$
	B-4	$$\frac{d[IL6-IL6R-JAK]c}{dt}=k_1[IL6]j[IL6R-JAK]c-k_{-1}[IL6-IL6R-JAK]c$$ $$\frac{d[IL6]j}{dt}=(-k_1[IL6]j[IL6R-JAK]c+k_{-1}[IL6-IL6R-JAK]c)\frac{1}{r}$$ $$\frac{d[IL6R-JAK]c}{dt}=-k_1[IL6]j[IL6R-JAK]c+k_{-1}[IL6-IL6R-JAK]c$$	$k_1=2x10^6$ $k_{-1}=0.02$ $K_d=10nM$ $r=30$
	B-5	$$\frac{d[IL6-IL6R-JAKP]c}{dt}=r_p[IL6-IL6R-JAK]c$$ $$\frac{d[IL6-IL6R-JAK]c}{dt}=-r_p[IL6-IL6R-JAK]c$$	$r_p=0.3$

	B-6	$\frac{d[IL6-IL6R-JAKP-STAT3]c}{dt} = k_1[IL6-IL6R-JAKP]c[STAT3]c - k_{-1}[IL6-IL6R-JAKP-STAT3]c$ $\frac{d[IL6-IL6R-JAKP]c}{dt} = -k_1[IL6-IL6R-JAKP]c[STAT3]c + k_{-1}[IL6-IL6R-JAKP-STAT3]c$ $\frac{d[STAT3]c}{dt} = -k_1[IL6-IL6R-JAKP]c[STAT3]c + k_{-1}[IL6-IL6R-JAKP-STAT3]c$	k_1=8x10^6 k_{-1}=0.8 K_d=100nM
	B-7	$\frac{d[IL6-IL6R-JAKP-STAT3P]c}{dt} = r_p[IL6-IL6R-JAKP-STAT3]c$ $\frac{d[IL6-IL6R-JAKP-STAT3]c}{dt} = -r_p[IL6-IL6R-JAKP-STAT3]c$	r_p=2
	B-8	$\frac{d[IL6-IL6R-JAKP-STAT3P]c}{dt} = k_1[IL6-IL6R-JAKP]c[STAT3P]c - k_{-1}[IL6-IL6R-JAKP-STAT3P]c$ $\frac{d[IL6-IL6R-JAKP]c}{dt} = -k_1[IL6-IL6R-JAKP]c[STAT3P]c + k_{-1}[IL6-IL6R-JAKP-STAT3P]c$ $\frac{d[STAT3P]c}{dt} = -k_1[IL6-IL6R-JAKP]c[STAT3P]c + k_{-1}[IL6-IL6R-JAKP-STAT3P]c$	k_1=5x10^6 k_{-1}=0.5 K_d=100nM

	B-9	$\frac{d[STAT3P-STAT3P]c}{dt} = k_1([STAT3P]c)^2 - k_{-1}[STAT3P-STAT3P]c$ $\frac{d[STAT3P]c}{dt} = 2(-k_1([STAT3P]c)^2 + k_{-1}[STAT3P-STAT3P]c)$	k_1=2x10^7 k_{-1}=0.1 K_d=5nM
	B-10	$\frac{d[STAT3P-STAT3P]n}{dt} = r_m[STAT3P-STAT3P]c$ $\frac{d[STAT3P-STAT3P]c}{dt} = -r_m[STAT3P-STAT3P]c$	r_m=0.1
	B-11	$\frac{d[IL6-IL6R-JAKP-SHP]c}{dt} = k_1[IL6-IL6R-JAKP]c[SHP]c - k_{-1}[IL6-IL6R-JAKP-SHP]c$ $\frac{d[IL6-IL6R-JAKP]c}{dt} = -k_1[IL6-IL6R-JAKP]c[SHP]c + k_{-1}[IL6-IL6R-JAKP-SHP]c$ $\frac{d[SHP]c}{dt} = -k_1[IL6-IL6R-JAKP]c[SHP]c + k_{-1}[IL6-IL6R-JAKP-SHP]c$	k_1=10^6 k_{-1}=0.2 K_d=200nM
	B-12	$\frac{d[IL6-IL6R-JAK-SHP]c}{dt} = r_d[IL6-IL6R-JAKP-SHP]c$ $\frac{d[IL6-IL6R-JAKP-SHP]c}{dt} = -r_d[IL6-IL6R-JAKP-SHP]c$	r_d=0.2

	B-13	$\frac{d[IL6-IL6R-JAK-SHP]c}{dt} = k_1[IL6-IL6R-JAK]c[SHP]c - k_{-1}[IL6-IL6R-JAK-SHP]c$ $\frac{d[IL6-IL6R-JAK]c}{dt} = -k_1[IL6-IL6R-JAK]c[SHP]c + k_{-1}[IL6-IL6R-JAK-SHP]c$ $\frac{d[SHP]c}{dt} = -k_1[IL6-IL6R-JAK]c[SHP]c + k_{-1}[IL6-IL6R-JAK-SHP]c$	$k_1=10^5$ $k_{-1}=0.2$ $K_d=2\mu M$
	B-14	$\frac{d[PPX-STAT3P]c}{dt} = k_1[PPX]c[STAT3P]c - k_{-1}[PPX-STAT3P]c$ $\frac{d[PPX]c}{dt} = -k_1[PPX]c[STAT3P]c + k_{-1}[PPX-STAT3P]c$ $\frac{d[STAT3P]c}{dt} = -k_1[PPX]c[STAT3P]c + k_{-1}[PPX-STAT3P]c$	$k_1=10^6$ $k_{-1}=0.2$ $K_d=200nM$
	B-15	$\frac{d[PPX-STAT3]c}{dt} = r_d[PPX-STAT3P]c$ $\frac{d[PPX-STAT3P]c}{dt} = -r_d[PPX-STAT3P]c$	$r_d=0.2$
	B-16	$\frac{d[PPX-STAT3]c}{dt} = k_1[PPX]c[STAT3]c - k_{-1}[PPX-STAT3]c$ $\frac{d[PPX]c}{dt} = -k_1[PPX]c[STAT3]c + k_{-1}[PPX-STAT3]c$ $\frac{d[STAT3]c}{dt} = -k_1[PPX]c[STAT3]c + k_{-1}[PPX-STAT3]c$	$k_1=10^4$ $k_{-1}=0.2$ $K_d=20\mu M$

	B-17	$\frac{d[STAT3P-STAT3P]n}{dt} = k_1([STAT3P]n)^2 - k_{-1}[STAT3P-STAT3P]n$ $\frac{d[STAT3P]n}{dt} = 2(-k_1([STAT3P]n)^2 + k_{-1}[STAT3P-STAT3P]n)$	k_1=2x10^7 k_{-1}=0.1 K_d=5nM
	B-18	$\frac{d[PPN-STAT3P]n}{dt} = k_1[PPN]n[STAT3P]n - k_{-1}[PPN-STAT3P]n$ $\frac{d[PPN]n}{dt} = -k_1[PPN]n[STAT3P]n + k_{-1}[PPN-STAT3P]n$ $\frac{d[STAT3P]n}{dt} = -k_1[PPN]n[STAT3P]n + k_{-1}[PPN-STAT3P]n$	k_1=10^6 k_{-1}=0.2 K_d=200nM
	B-19	$\frac{d[PPN-STAT3]n}{dt} = r_d[PPN-STAT3P]n$ $\frac{d[PPN-STAT3P]n}{dt} = -r_d[PPN-STAT3P]n$	r_d=0.3
	B-20	$\frac{d[PPN-STAT3]n}{dt} = k_1[PPN]n[STAT3]n - k_{-1}[PPN-STAT3]n$ $\frac{d[PPN]n}{dt} = -k_1[PPN]n[STAT3]n + k_{-1}[PPN-STAT3]n$ $\frac{d[STAT3]n}{dt} = -k_1[PPN]n[STAT3]n + k_{-1}[PPN-STAT3]n$	k_1=10^4 k_{-1}=0.2 K_d=20μM

	B-21	$\frac{d[STAT3]c}{dt} = r_m[STAT3]n$ $\frac{d[STAT3]n}{dt} = -r_m[STAT3]n$	r_m=0.3
	B-22	$\frac{d[SOCS]c}{dt} = r_s[NFkBP - STAT3P - STAT3P]n$	r_s=0.002
	B-23	$\frac{d[SOCS]c}{dt} = r_s[STAT3P - STAT3P]n$	r_s=0.0004
	B-24	$\frac{d[IL6 - IL6R - JAKP - SOCS]c}{dt} = k_1[IL6 - IL6R - JAKP]c[SOCS]c - k_{-1}[IL6 - IL6R - JAKP - SOCS]c$ $\frac{d[IL6 - IL6R - JAKP]c}{dt} = -k_1[IL6 - IL6R - JAKP]c[SOCS]c + k_{-1}[IL6 - IL6R - JAKP - SOCS]c$ $\frac{d[SOCS]c}{dt} = -k_1[IL6 - IL6R - JAKP]c[SOCS]c + k_{-1}[IL6 - IL6R - JAKP - SOCS]c$	k_1=10^8 k_{-1}=1 K_d=10nM
IL-6 production	BA-1	$\frac{d[mRNAIL6]n}{dt} = k_f \frac{[NFkBP - STAT3P - STAT3P]n}{K_t + [NFkBP - STAT3P - STAT3P]n}$	k_f=2x10^{-12} Kt=200nM
	BA-2	$\frac{d[mRNAIL6]c}{dt} = r_m[mRNAIL6]n$ $\frac{d[mRNAIL6]n}{dt} = -r_m[mRNAIL6]n$	r_m=0.02

	BA-3	$\frac{d[IL6]e}{dt} = r_s[mRNAIL6]c$	r_s=0.02
	BA-4	$\frac{d[IL6]j}{dt} = (r_m[IL6]e)\frac{1}{r}$ $\frac{d[IL6]e}{dt} = -r_m[IL6]e$	r_m=0.03 r=30
IL-6 receptor production	BB-1	$\frac{d[mRNAIL6R]n}{dt} = k_f \frac{[NFkBP-STAT3P-STAT3P]n}{K_t + [NFkBP-STAT3P-STAT3P]n}$	k_f=2x10^{-12} Kt=200nM
	BB-2	$\frac{d[mRNAIL6R]c}{dt} = r_m[mRNAIL6R]n$ $\frac{d[mRNAIL6R]n}{dt} = -r_m[mRNAIL6R]n$	r_m=0.02
	BB-3	$\frac{d[IL6R]e}{dt} = r_s[mRNAIL6R]c$	r_s=0.02
	BB-4	$\frac{d[IL6R]c}{dt} = r_m[IL6R]e$ $\frac{d[IL6R]e}{dt} = -r_m[IL6R]e$	r_m=0.002

IL-6 receptor internalization	BC-1	$\frac{d[IL6R]i}{dt} = r_i\left(e_1 + (1-e_1)\left(1 - e^{\frac{-3t}{T_1}}\right)\right)[IL6R]c$ $\frac{d[IL6R]c}{dt} = -r_i\left(e_1 + (1-e_1)\left(1 - e^{\frac{-3t}{T_1}}\right)\right)[IL6R]c$	r_i=0.00016 e_1=0.12 T_1=35
	BC-2	$\frac{d[IL6R-JAK]i}{dt} = r_i\left(e_1 + (1-e_1)\left(1 - e^{\frac{-3t}{T_1}}\right)\right)[IL6R-JAK]c$ $\frac{d[IL6R-JAK]c}{dt} = -r_i\left(e_1 + (1-e_1)\left(1 - e^{\frac{-3t}{T_1}}\right)\right)[IL6R-JAK]c$	r_i=0.0024 e_1=0.12 T_1=35
	BC-3	$\frac{d[IL6-IL6R-JAK]i}{dt} = r_i\left(e_1 + (1-e_1)\left(1 - e^{\frac{-3t}{T_1}}\right)\right)[IL6-IL6R-JAK]c$ $\frac{d[IL6-IL6R-JAK]c}{dt} = -r_i\left(e_1 + (1-e_1)\left(1 - e^{\frac{-3t}{T_1}}\right)\right)[IL6-IL6R-JAK]c$	r_i=0.012 e_1=0.12 T_1=35
	BC-4	$\frac{d[IL6-IL6R-JAKP]i}{dt} = r_i\left(e_1 + (1-e_1)\left(1 - e^{\frac{-3t}{T_1}}\right)\right)[IL6-IL6R-JAKP]c$ $\frac{d[IL6-IL6R-JAKP]c}{dt} = -r_i\left(e_1 + (1-e_1)\left(1 - e^{\frac{-3t}{T_1}}\right)\right)[IL6-IL6R-JAKP]c$	r_i=0.004 e_1=0.12 T_1=35
	BC-5	$\frac{d[IL6R]c}{ct} = r_m[IL6R]i$ $\frac{d[IL6R]i}{ct} = -r_m[IL6R]i$	r_m=0.0012

NFkB-STAT3 complex formation	C-1	$\frac{d[NFkBP-STAT3P-STAT3P]c}{dt}$ $= k_1[NFkBP]c[STAT3P-STAT3P]c - k_{-1}[NFkBP-STAT3P-STAT3P]c$ $\frac{d[NFkBP]c}{dt} = -k_1[NFkBP]c[STAT3P-STAT3P]c + k_{-1}[NFkBP-STAT3P-STAT3P]c$ $\frac{d[STAT3P-STAT3P]c}{dt}$ $= -k_1[NFkBP]c[STAT3P-STAT3P]c + k_{-1}[NFkBP-STAT3P-STAT3P]c$	k_1=2x10^9 k_{-1}=100 K_d=50nM
	C-1b	$\frac{d[NFkBP-STAT3P-STAT3P]n}{dt}$ $= k_1[NFkBP]n[STAT3P-STAT3P]n - k_{-1}[NFkBP-STAT3P-STAT3P]n$ $\frac{d[NFkBP]n}{dt} = -k_1[NFkBP]n[STAT3P-STAT3P]n + k_{-1}[NFkBP-STAT3P-STAT3P]n$ $\frac{d[STAT3P-STAT3P]n}{dt}$ $= -k_1[NFkBP]n[STAT3P-STAT3P]n + k_{-1}[NFkBP-STAT3P-STAT3P]n$	k_1=2x10^9 k_{-1}=100 K_d=50nM
	C-2	$\frac{d[NFkBP-STAT3P-STAT3P]n}{dt} = r_m[NFkBP-STAT3P-STAT3P]c$ $\frac{d[NFkBP-STAT3P-STAT3P]c}{dt} = -r_m[NFkBP-STAT3P-STAT3P]c$	r_m=0.00005

	C-3	$\frac{d[NFkBP-STAT3P-STAT3P]c}{dt} = r_m[NFkBP-STAT3P-STAT3P]n$ $\frac{d[NFkBP-STAT3P-STAT3P]n}{dt} = -r_m[NFkBP-STAT3P-STAT3P]n$	r_m=0.00005
cytokine production	D-1	$\frac{d[epiregulin]j}{dt} = (r_s[synovial]j)\frac{[NFkBP-STAT3P-STAT3P]n}{K_t+[NFkBP-STAT3P-STAT3P]n}$	r_s=800 K_t=5nM
	D-2	$\frac{d[CCL2]j}{dt} = (r_s[synovial]j)\frac{[NFkBP-STAT3P-STAT3P]n}{K_t+[NFkBP-STAT3P-STAT3P]n}$	r_s=100 K_t=5nM
	D-3	$\frac{d[CCL20]j}{dt} = (r_s[synovial]j)\frac{[NFkBP-STAT3P-STAT3P]n}{K_t+[NFkBP-STAT3P-STAT3P]n}$	r_s=20 K_t=5nM
	D-4	$\frac{d[IL-17]j}{dt} = r_s[Th17]j$	r_s=100
	D-5	$\frac{d[IL6]j}{dt} = r_s[macrophage]j$	r_s=400
	D-6	$\frac{d[TNF]j}{dt} = r_s[macrophage]j$	r_s=10
	D-7	$\frac{d[CCL20]j}{dt} = r_s[macrophage]j$	r_s=20
cell movement	E-1	$\frac{d[Th17]j}{dt} = (r_m[Th17]b)\frac{[CCL20]j}{K_m+[CCL20]j}$	r_m=0.00012 K_m=10nM
	E-2	$\frac{d[macrophage]j}{dt} = (r_m[macrophage]b)\frac{[CCL2]j}{K_m+[CCL2]j}$	r_m=0.00012 K_m=10nM

proliferation	F-1	$\frac{d[synovial]j}{dt} = (r_l[synovial]j)(r + (1-r)\frac{[epiregulin]j}{K_{m1}+[epiregulin]j})\frac{[NFkBP-STAT3P-STAT3P]n}{K_{m2}+[NFkBP-STAT3P-STAT3P]n}$	r_l=0.0002 K_{m1}=1nM r=0.6 K_{m2}=5nM
cell death	G-1	$\frac{d[synovial]j}{dt} = (-r_e[synovial]j)(r + (1-r)\frac{[synovial]j}{K_m+[synovial]j})$	r_e=0.0006 K_m=20fM r=0.07
	G-2	$\frac{d[Th17]j}{dt} = (-r_e[Th17]j)\left(r + (1-r)\frac{[Th17]j}{K_m+[Th17]j}\right)$	r_e=0.0004 K_m=20fM r=0.1
	G-3	$\frac{d[macrophage]j}{dt} = (-r_e[macrophage]j)\left(r + (1-r)\frac{[macrophage]j}{K_m+[macrophage]j}\right)$	r_e=0.0002 K_m=20fM r=0.1
degradation	H-1	$\frac{d[IkBaP]c}{dt} = -r_e[IkBaP]c$	r_e=0.005
	H-2	$\frac{d[IKKP]c}{dt} = -r_e[IKKP]c$	r_e=0.005
	H-3	$\frac{d[IL-17]j}{dt} = -r_e[IL-17]j$	r_e=0.00002
	H-4	$\frac{d[TNF]j}{dt} = -r_e[TNF]j$	r_e=0.0005
	H-5	$\frac{d[IL6]j}{dt} = -r_e[IL6]j$	r_e=0.00004

	H-6	$\frac{d[epiregulin]j}{dt} = -r_e[epiregulin]j$	r_e=0.0005
	H-7	$\frac{d[mRNAIL6]c}{dt} = -r_e[mRNAIL6]c$	r_e=0.001
	H-8	$\frac{d[mRNAIL6R]c}{dt} = -r_e[mRNAIL6R]c$	r_e=0.0005
	H-9	$\frac{d[IL6R]i}{dt} = -r_e[IL6R]i$	r_e=0.00005
	H-10	$\frac{d[SOCS]c}{dt} = -r_e[SOCS]c$	r_e=0.0005
	H-11	$\frac{d[CCL2]j}{dt} = -r_e[CCL2]j$	r_e=0.0002
	H-12	$\frac{d[CCL20]j}{dt} = -r_e[CCL20]j$	r_e=0.0005
Initial concentration		[synovial]j	$1.204x10^6$ cells/ml = 2 fM
		[Th17]b	$1.204x10^6$ cells/ml = 2 fM
		[macrophage]b	$1.204x10^6$ cells/ml = 2 fM

		[NFkB]c	0.2 nM
		[IkBa]c	100 nM
		[NFkB-IkBa]c	200 nM
		[IL6]j	1 pM
		[IL6R]c	4 nM
		[JAK]c	8 nM
		[STAT3]c	800 nM
		[SHP]c	100 nM
		[PPX]c	50 nM
		[PPN]n	60 nM
		[CCL20]j	2 nM
		[CCL2]j	0.5 nM

The [x]b, [x]j, [x]c, [x]n , [x]e, and [x]i indicate the concentration of factor x in blood, joint, cytoplasm of synovial cells, nucleus of synovial cell, ER of synovial cells, and internalized receptors, respectively.

k_f, K_m, k_1, k_{-1}, K_d, r_p, r_d, r_m, K_t, r_s, r_i, r_l, and r_e denote the rate constant for production, the dissociation constant for cytokine, the rate constnt for binding, the rate constant for dissociation, the dissociation constant, the rate constant for phosphorylation, the rate constant for dephosphorylation, the rate constant for movement, the dissociation constant for transcription, the rate constant for synthesis, the rate constant for internalization, the rate constant for proliferation, and the rate constant for degradation, respectively.

In F759 cells, reaction “B-24” is excluded.

In this system, the base time unit is minute.

The initial concentrations of all other factors are 0.

Figure 1.

A

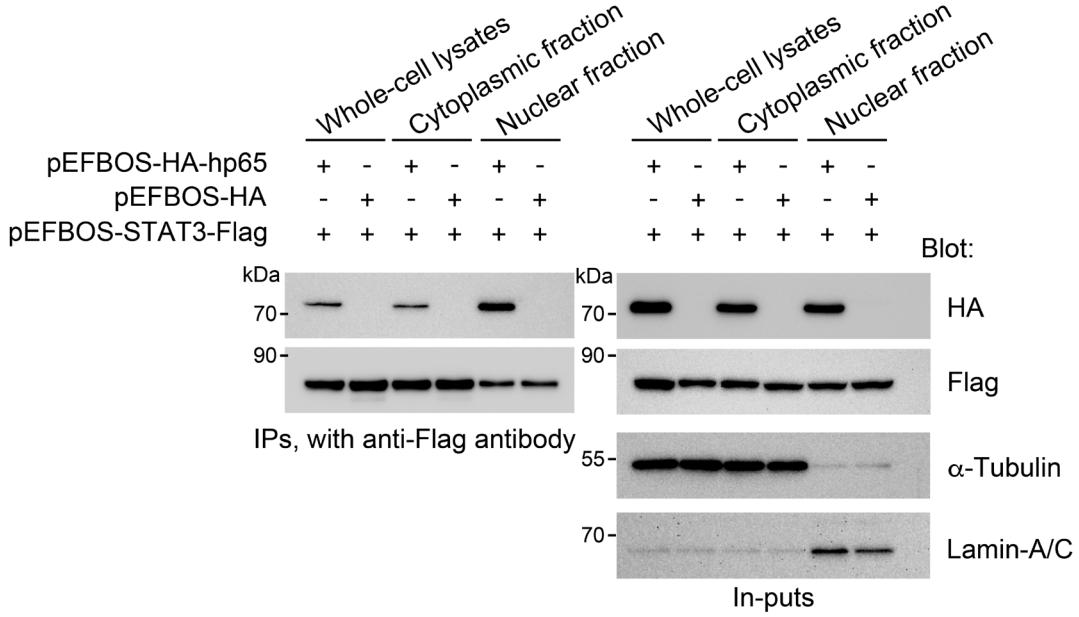

B

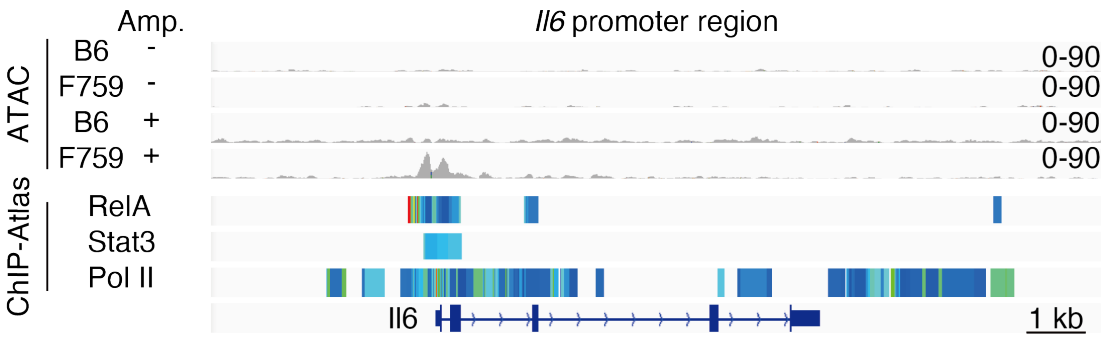

C

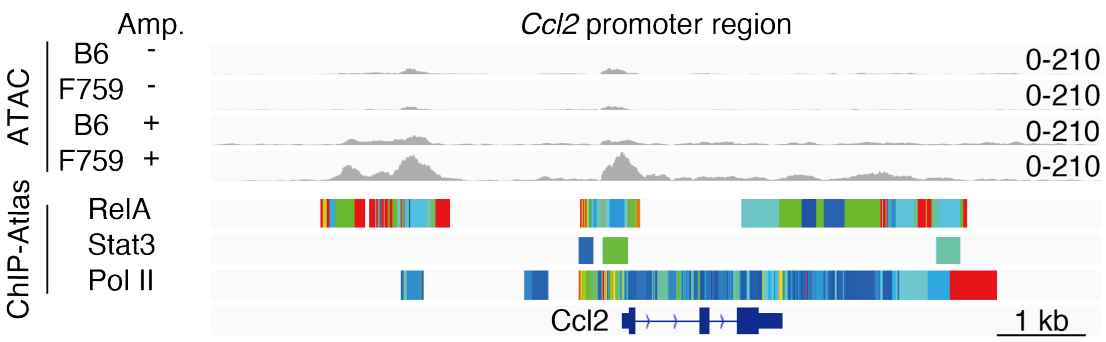

D

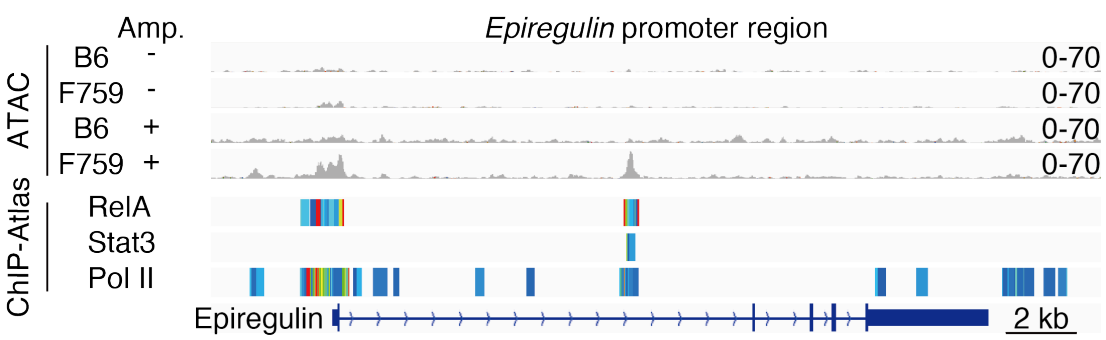

Figure 2.

A

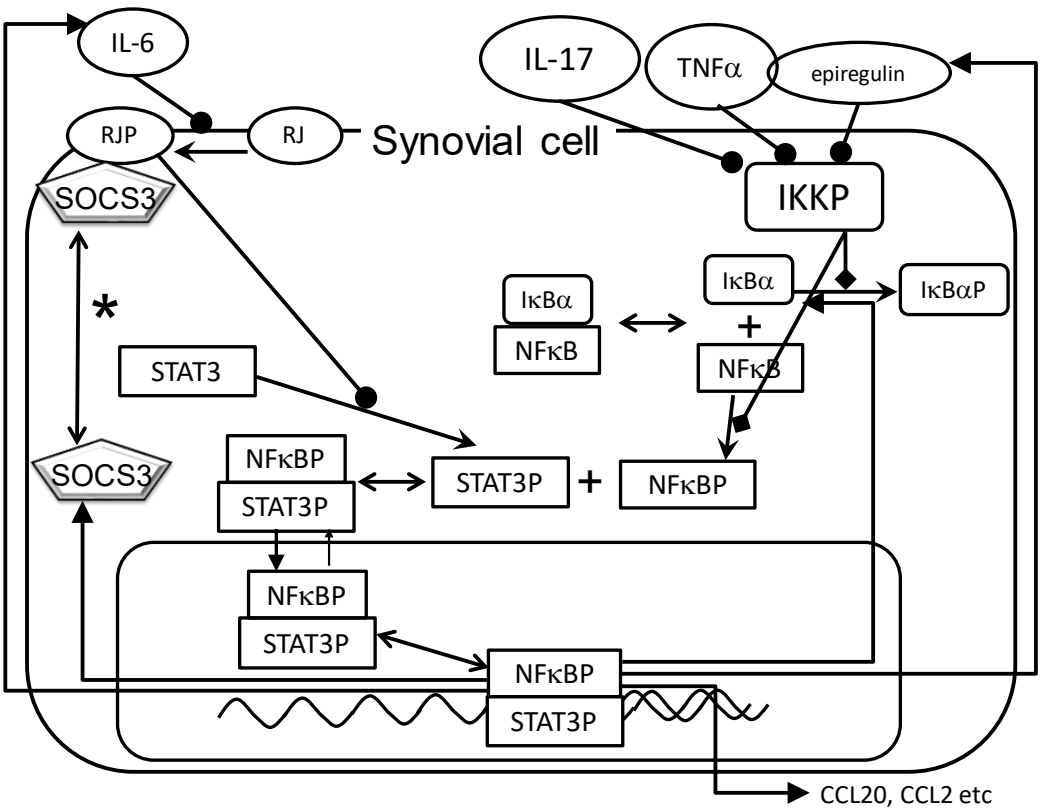
IL-6
IL-17
TNFα
epiregulin
RJP
RJ
Synovial cell
SOCS3
IKKP
IκBα
IκBαP
NFκB
STAT3
NFκBP
STAT3P
CCL20, CCL2 etc

B

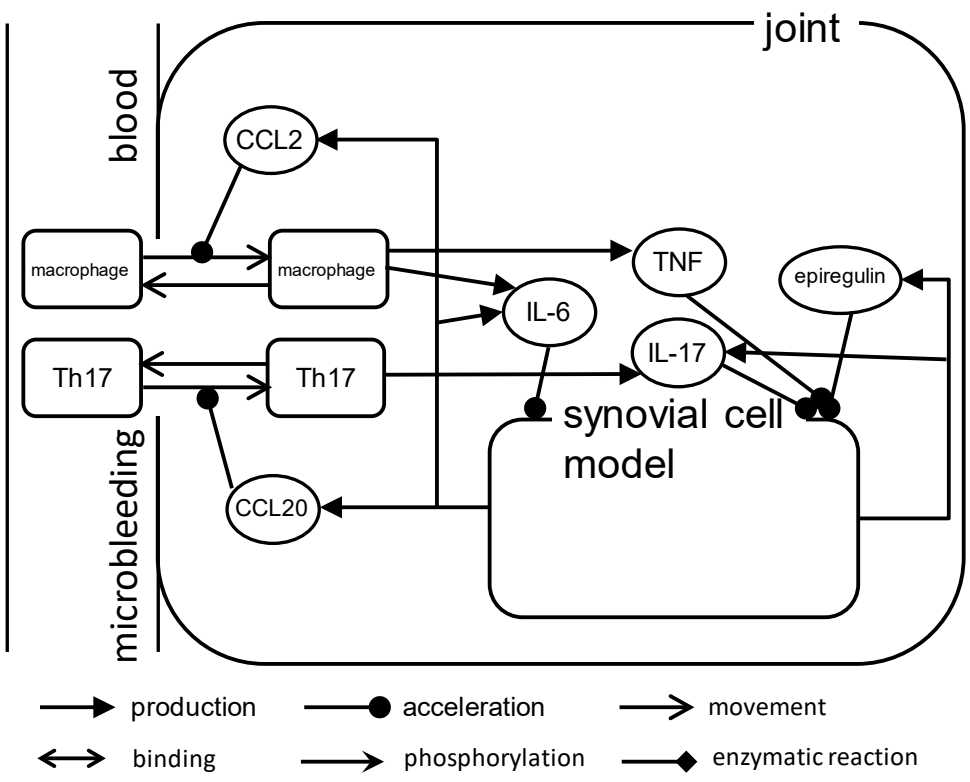
joint
blood
CCL2
macrophage
macrophage
TNF
epiregulin
IL-6
IL-17
Th17
Th17
synovial cell
model
CCL20
microbleeding
production
acceleration
movement
binding
phosphorylation
enzymatic reaction

Figure 3.

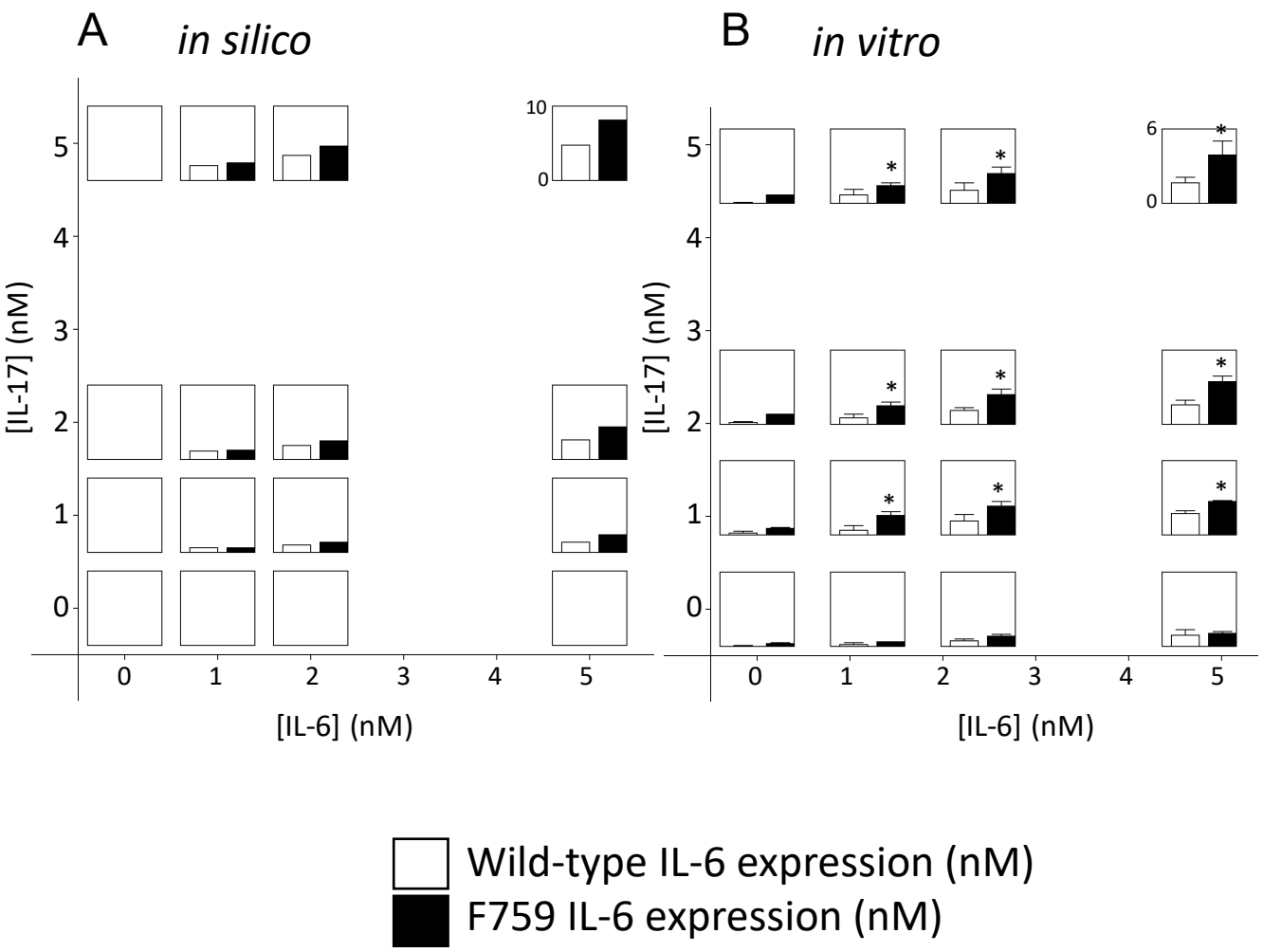

Wild-type IL-6 expression (nM)

F759 IL-6 expression (nM)

Figure 4.

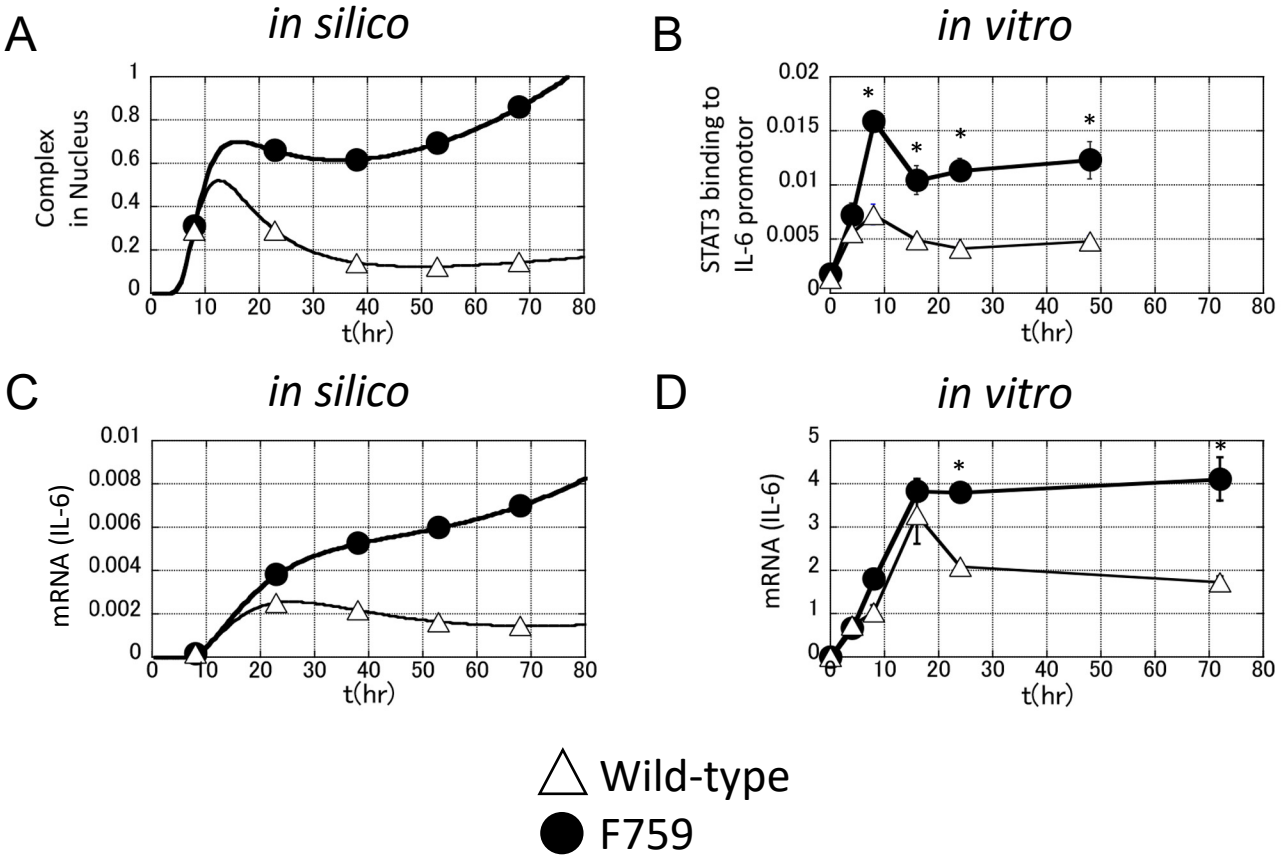
A
in silico
Complex in Nucleus
t(hr)
B
in vitro
STAT3 binding to IL-6 promotor
t(hr)
C
in silico
mRNA (IL-6)
t(hr)
D
in vitro
mRNA (IL-6)
t(hr)
Wild-type
F759

Figure 5.

A *in silico*

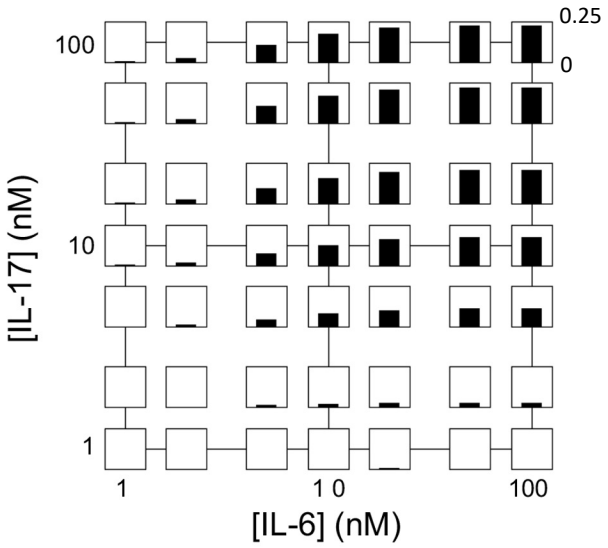

in the presence of
STAT3/NFkB complex

B *in silico*

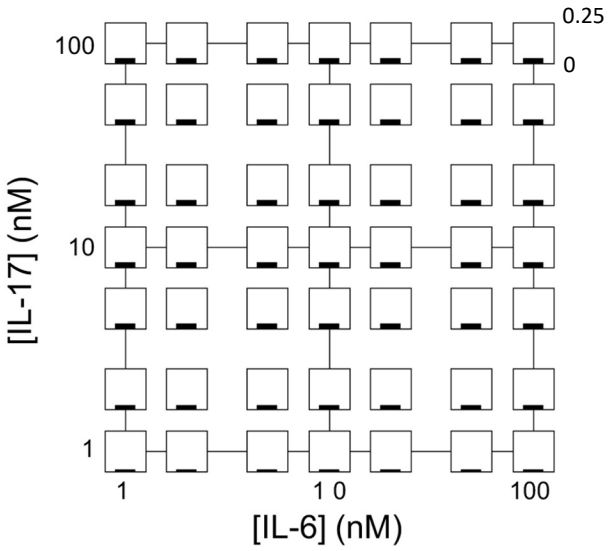

in the absence of
STAT3/NFkB complex

IL-6 expression (nM)

Figure 6.

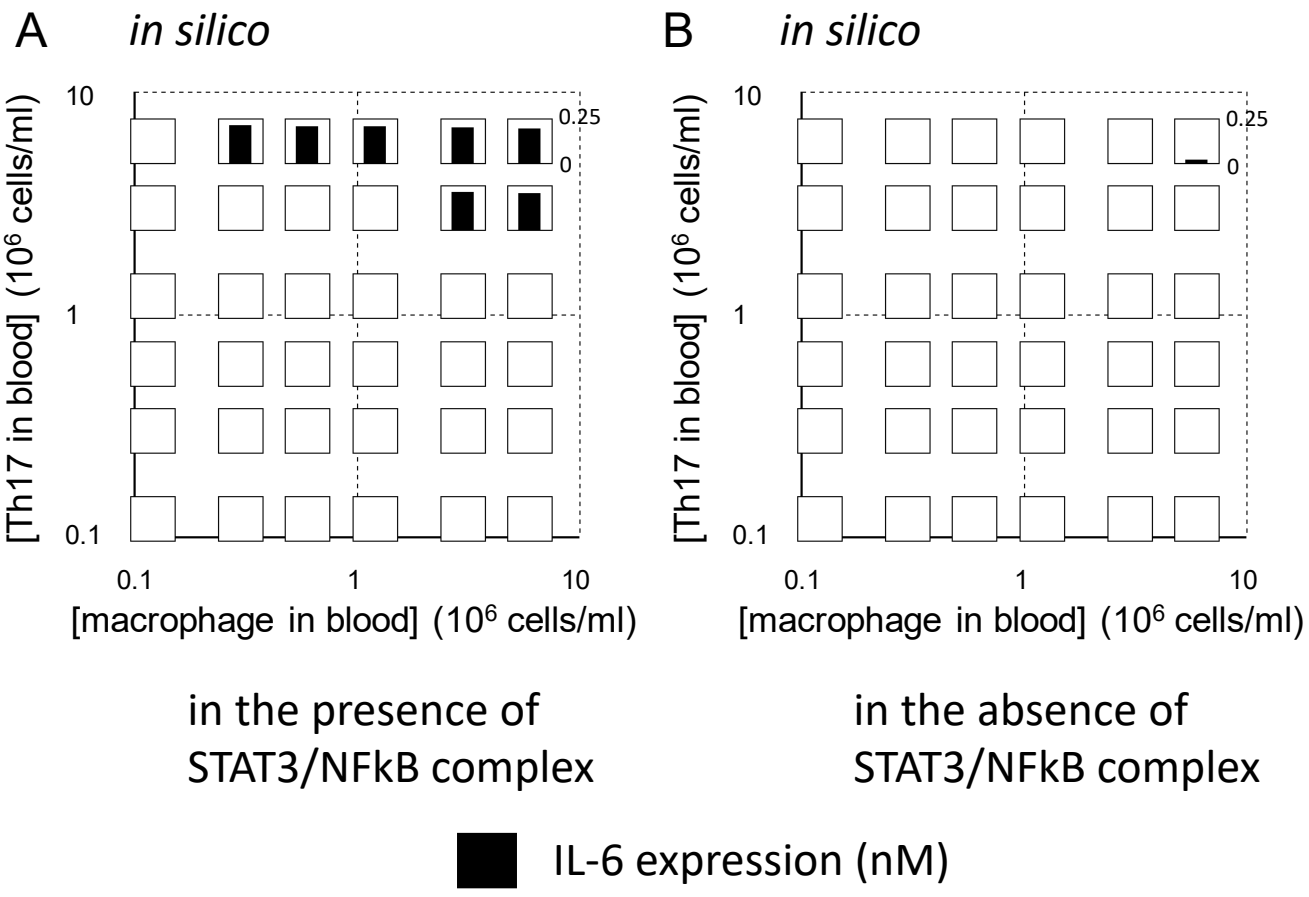
A
in silico
B
in silico
10
1
0.1
0.25
0
[Th17 in blood] (10^6 cells/ml)
0.1
1
10
[macrophage in blood] (10^6 cells/ml)
in the presence of
STAT3/NFkB complex
in the absence of
STAT3/NFkB complex
IL-6 expression (nM)

Figure 7.

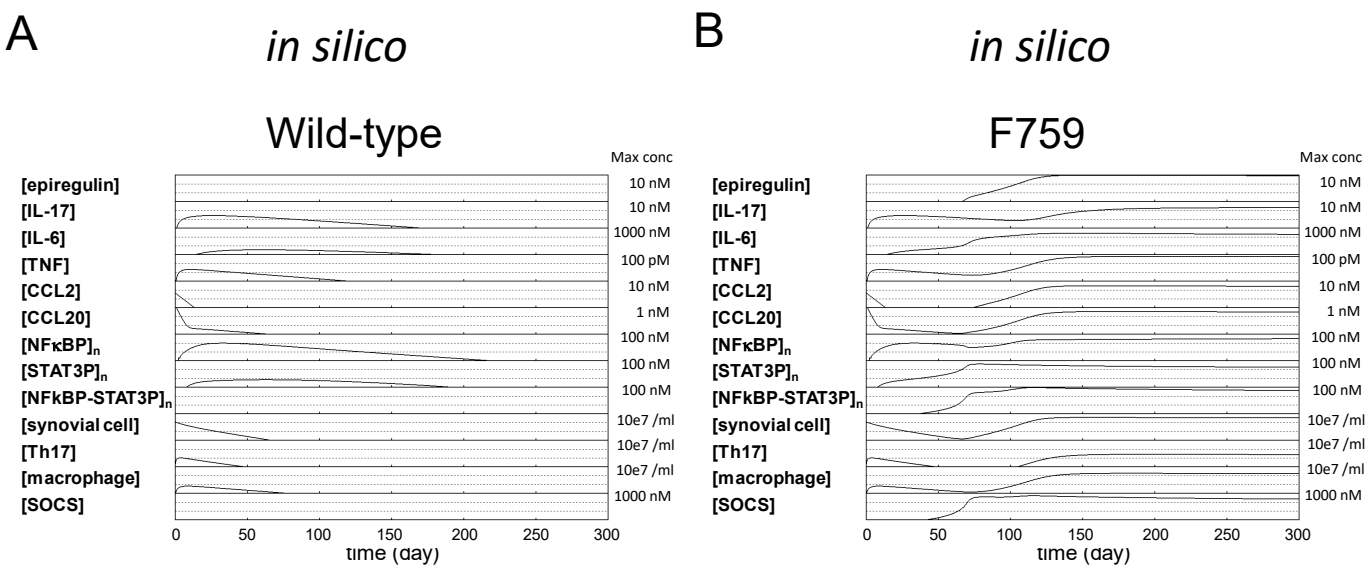
A
in silico
Wild-type
Max conc
[epiregulin]
[IL-17]
[IL-6]
[TNF]
[CCL2]
[CCL20]
[NFκBP]n
[STAT3P]n
[NFkBP-STAT3P]n
[synovial cell]
[Th17]
[macrophage]
[SOCS]
10 nM
10 nM
1000 nM
100 pM
10 nM
1 nM
100 nM
100 nM
100 nM
10e7 /ml
10e7 /ml
10e7 /ml
1000 nM
0
50
100
150
200
250
300
time (day)
B
in silico
F759
Max conc
[epiregulin]
[IL-17]
[IL-6]
[TNF]
[CCL2]
[CCL20]
[NFκBP]n
[STAT3P]n
[NFkBP-STAT3P]n
[synovial cell]
[Th17]
[macrophage]
[SOCS]
10 nM
10 nM
1000 nM
100 pM
10 nM
1 nM
100 nM
100 nM
100 nM
10e7 /ml
10e7 /ml
10e7 /ml
1000 nM
0
50
100
150
200
250
300
time (day)

Figure 8.

A F759 w/o Ab

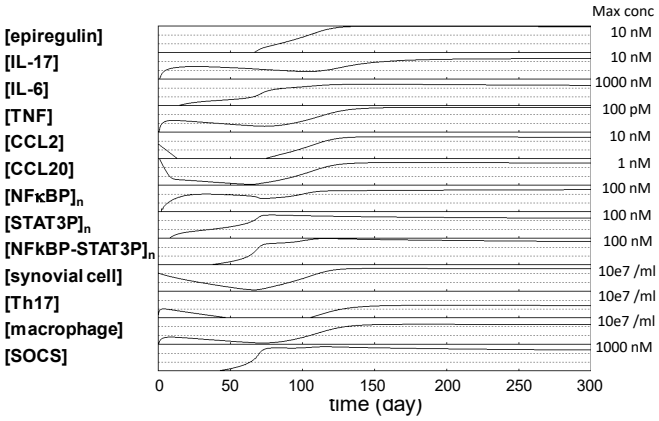

B F759+anti-IL6 Ab at day 250

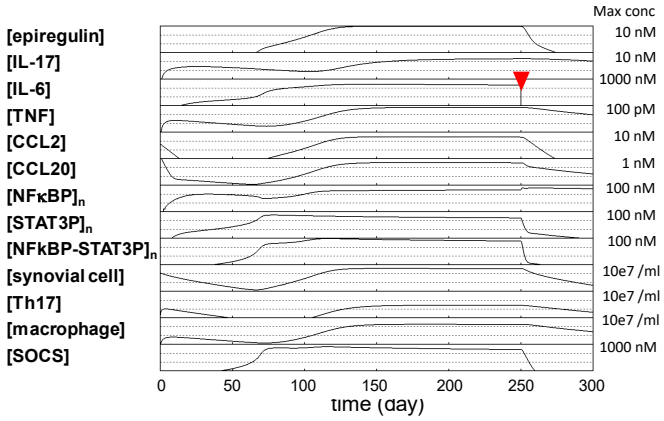

C F759+anti-TNF Ab at day 250

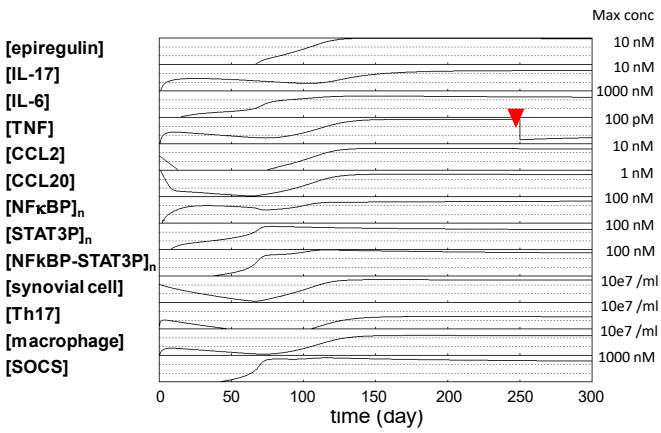

D F759+anti-IL17 Ab at day 250

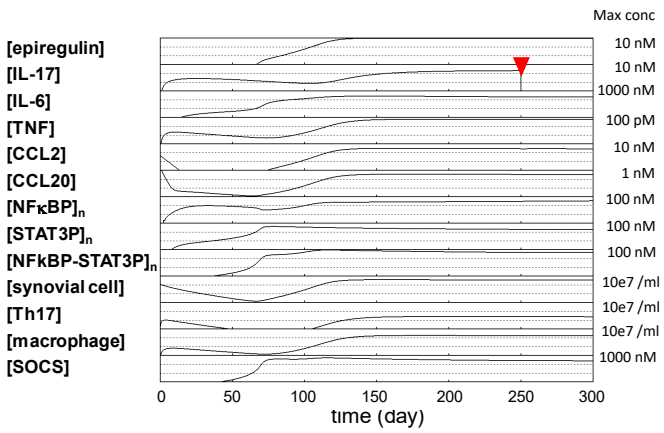

E F759+anti-IL17/TNF Abs at day 250

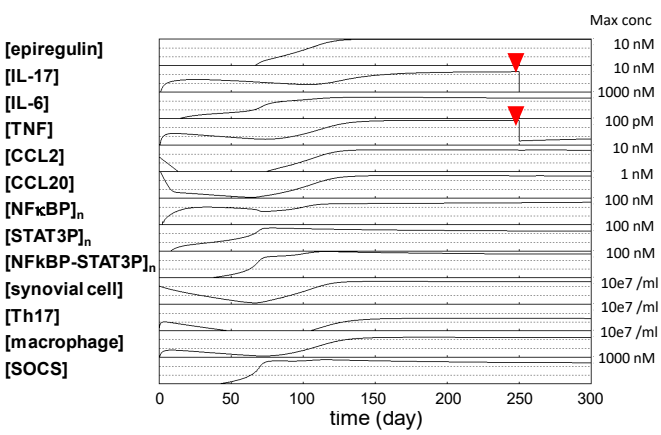

F

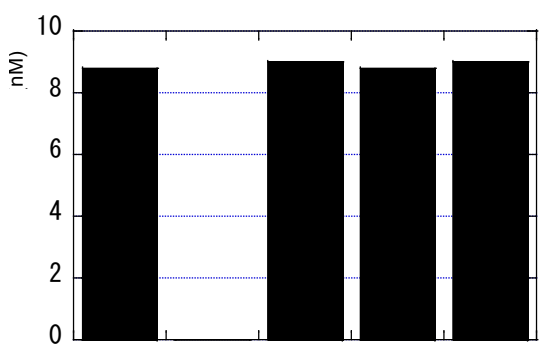

G F759+anti-IL17 Ab at day 50

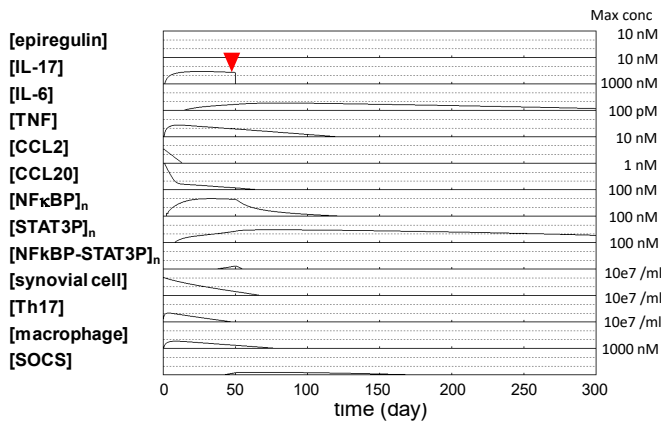

H F759+anti-IL17 Ab at day 100

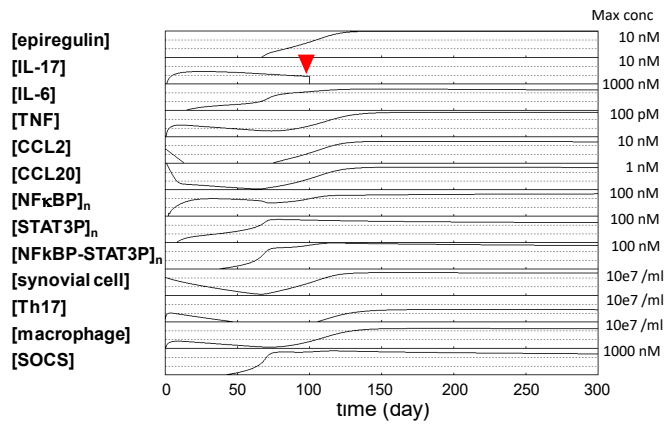

Figure 9.

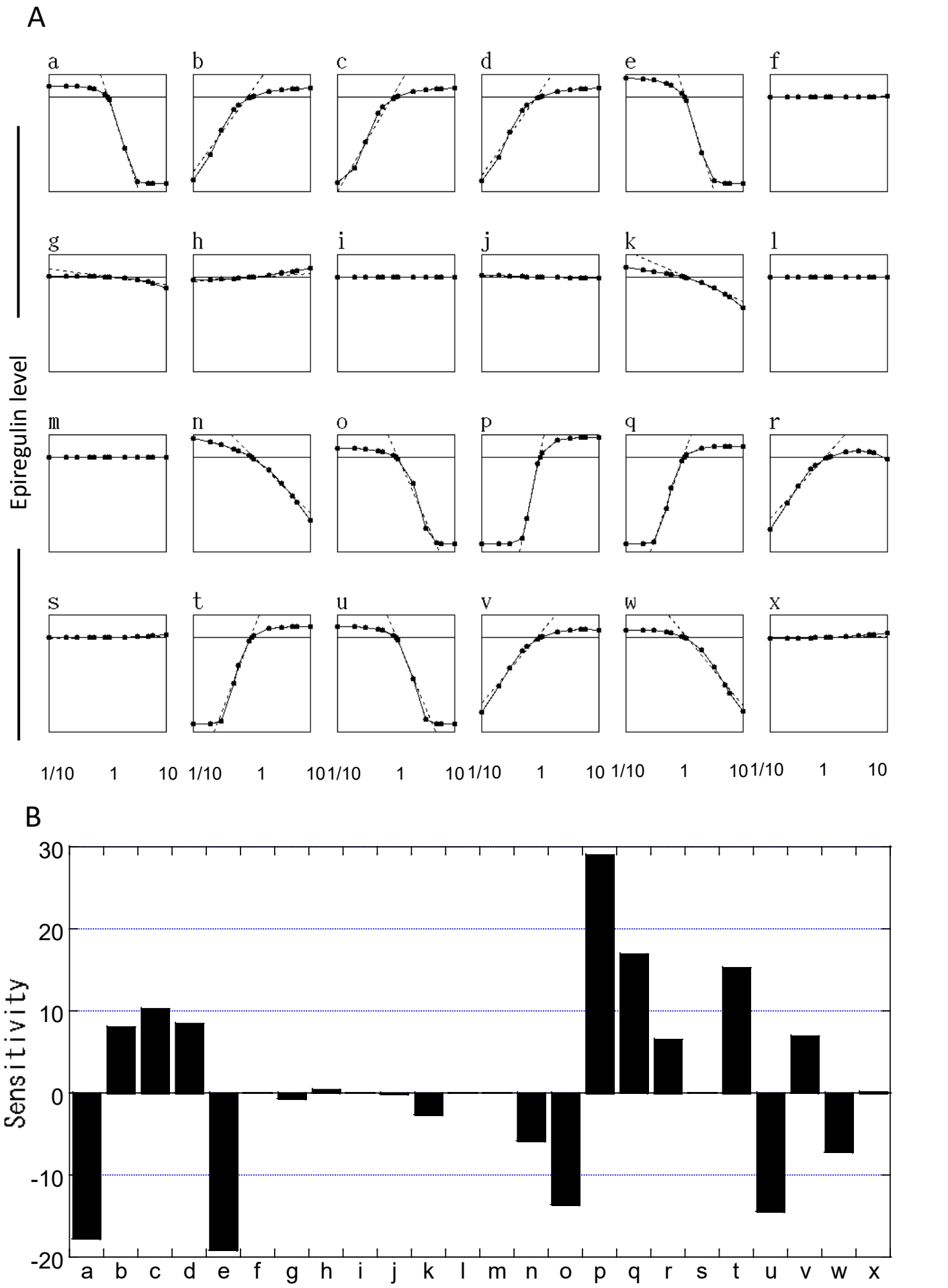
A
a
b
c
d
e
f
g
h
i
j
k
l
m
n
o
p
q
r
s
t
u
v
w
x
Epiregulin level
1/10
1
10
B
Sensitivity
30
20
10
0
-10
-20
a b c d e f g h i j k l m n o p q r s t u v w x

Supplementary Figure 1.